Conversion of Methanol to Hydrocarbons: How Zeolite Cavity and Pore Size Controls Product Selectivity

UNIVERSITÀ DEGLI STUDI DI TORINO

Conversion of Methanol to Hydrocarbons: How Zeolite Cavity and Pore Size Controls Product Selectivity

by

Olsbye U.; Svelle S.; Bjorgen M.; Beato P.; Janssens T.V.W.; Joensen F.; Bordiga S.; Lillerud K.P.

Angew. Chem. Int. Ed. **2012**, *51*, 5810 – 5831

DOI: 10.1002/anie.201103657

Review

Conversion of Methanol to Hydrocarbons: How Zeolite Cavity and Pore Size Controls Product Selectivity

Authors

- **Prof. Unni Olsbye,**
  Corresponding author
  - E-mail address: unni.olsbye@kjemi.uio.no
  2. Department of Chemistry inGAP Centre of Research-based Innovation, University of Oslo, P.O. Box 1033 Blindern, 0315 Oslo (Norway) http://www.mn.uio.no/ingap
  - Department of Chemistry inGAP Centre of Research-based Innovation, University of Oslo, P.O. Box 1033 Blindern, 0315 Oslo (Norway) http://www.mn.uio.no/ingap
- **Prof. Stian Svelle,**
  0. Department of Chemistry inGAP Centre of Research-based Innovation, University of Oslo, P.O. Box 1033 Blindern, 0315 Oslo (Norway) http://www.mn.uio.no/ingap
- **Prof. Morten Bjørgen,**
  0. Department of Chemistry, Norwegian University of Science and Technology, 7491 Trondheim (Norway)
- **Dr. Pablo Beato,**
  0. Haldor Topsøe, Nymøllevej 55, 2800 Kgs. Lyngby (Denmark)
- **Dr. Ton V. W. Janssens,**
  0. Haldor Topsøe, Nymøllevej 55, 2800 Kgs. Lyngby (Denmark)
- **Finn Joensen,**
  0. Haldor Topsøe, Nymøllevej 55, 2800 Kgs. Lyngby (Denmark)
- **Prof. Silvia Bordiga,**
  0. Department of Chemistry, NIS Centre of Excellence, University of Torino, Via P. Giuria 7, 10125 Turin (Italy)
- **Prof. Karl Petter Lillerud**
  0. Department of Chemistry inGAP Centre of Research-based Innovation, University of Oslo, P.O. Box 1033 Blindern, 0315 Oslo (Norway) http://www.mn.uio.no/ingap

From the Contents

4. Deactivation by CarbonDeposition
5. Other Reactants
6. Recent Developments
7. Summary and Outlook

Abstract

Liquid hydrocarbon fuels play an essential part in the global energy chain, owing to their high energy density and easy transportability. Olefins play a similar role in the production of consumer goods. In a post-oil society, fuel and olefin production will rely on alternative carbon sources, such as biomass, coal, natural gas, and CO_2. The methanol-to-hydrocarbons (MTH) process is a key step in such routes, and can be tuned into production of gasoline-rich (methanol to gasoline; MTG) or olefin-rich (methanol to olefins; MTO) product mixtures by proper choice of catalyst and reaction conditions. This Review presents several commercial MTH projects that have recently been realized, and also fundamental research into the synthesis of microporous materials for the targeted variation of selectivity and lifetime of the catalysts.

1. Introduction

1.1. Industrial Applications

1.1.1. Methanol-to-Gasoline Process

The synthesis of H-ZSM-5 in the early 1970s along with the discovery of its unique catalytic properties by researchers at Mobil triggered an immense interest in industry and academia. Research and development gained additional momentum by the first and second oil crises in 1973 and 1979, and an extensive development program was initiated,[1] involving bench-scale and pilot-scale demonstration of the methanol-to-gasoline (MTG) synthesis. In addition to the fixed-bed process, a fluid-bed version, offering the advantage of excellent temperature control and continuous catalyst regeneration, was developed and demonstrated on a 4 bpd scale (barrels per day; 1 barrel=159 L) in Paulsboro, NJ, and on a 100 bpd scale during 1981–1984 in Wesseling, Germany.

In 1985, the MTG process was commercialized in New Zealand, where Mobil, in a partnership with the New Zealand government, built a 14 500 bpd plant based on natural gas, converted through synthesis gas into methanol.[2, 3] In the MTG process (see simplified block diagram in Figure 1) crude methanol is dehydrated over a slightly acidic catalyst (typically alumina-based) into an equilibrium mixture of methanol, dimethyl ether, and water before entering the gasoline synthesis loop. In the gasoline reactor, the feed mixture is converted into C_1–C_{11} hydrocarbons with C_{5+} (benzene fraction) selectivity of about 80 %. The reaction is strongly exothermic (56 kJ mol^{-1} CH_3OH; 45 kJ mol^{-1} MeOH–Me_2O–H_2O) and to control the temperature in the adiabatic reactor light hydrocarbons, hydrogen, and carbon oxides (formed in small amounts by cracking reactions) are recycled to dilute the feed. Typical inlet and exit temperatures are 350 and 410 °C and the pressure is around 20 bar. Despite the unique properties of H-ZSM-5, slow coke formation does take place and catalyst activity must be restored by controlled coke burn-off. Therefore, the MTG section consists of parallel reactors allowing for intermittent regeneration.

The gasoline from the MTG process consists of (predominantly iso-) paraffins, aromatics (predominantly methyl-substituted), naphthenes, and olefins. Among the aromatics, specifically 1,2,4,5-tetramethylbenzene (durene, formed in excessive amounts relative to the equilibrium among tetramethylbenzenes owing to the shape selectivity of H-ZSM-5) is a concern owing to its relatively high melting point (79 °C). Under most conditions up to about 4 %, durene is acceptable, but in cold climates, under winter conditions, it may foul the engine's fuel injection system and, unless the gasoline product is used as a blending agent in refineries, the heavy gasoline fraction must be subjected to hydroisomerization/transalkylation.

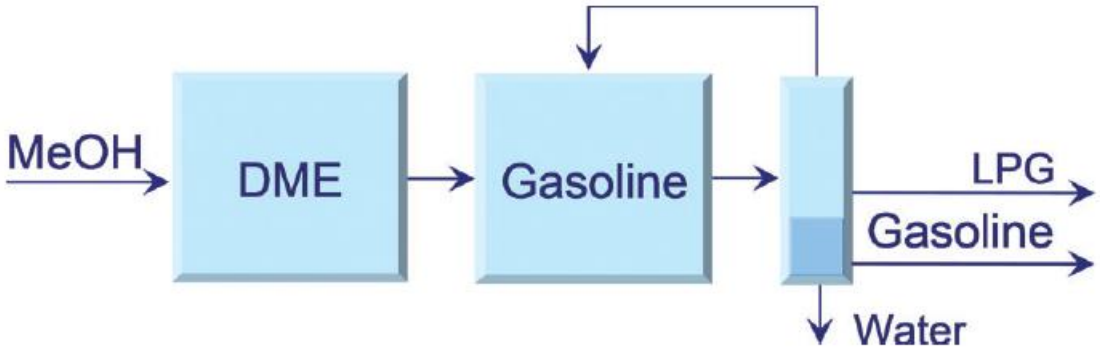

Figure 1. Methanol-to-gasoline (MTG) process: adiabatic dehydration reactor for DME synthesis and parallel adiabatic gasoline reactors. DME=dimethyl ether, LPG=liquified petroleum gas.

An alternative to the MTG route is the TIGAS process that was developed by Haldor Topsøe and demonstrated on a 1 tonne per day scale in the 1980s.[4] The process, outlined in Figure 2, merges the methanol, dimethyl ether (DME), and gasoline syntheses into a single loop without isolation of methanol. The TIGAS process exploits the synergy in integrating the methanol and dimethyl ether syntheses, leading to a significant enhancement in synthesis gas conversion and, thereby, improving process efficiency, primarily by reducing recycle rates and avoiding the condensation and re-evaporation of methanol.

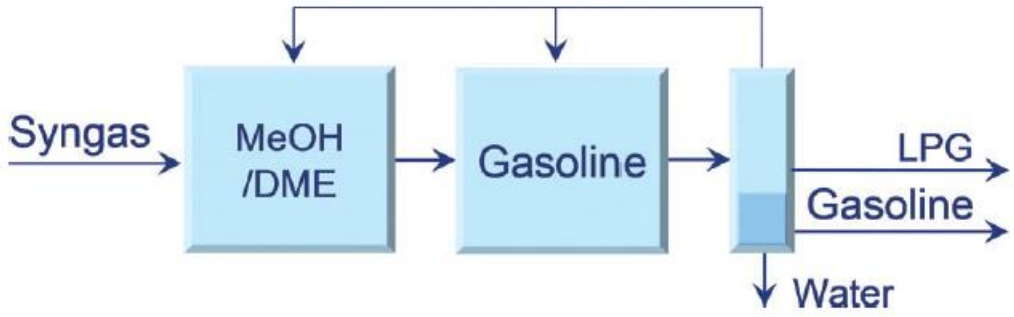

Figure 2. Syngas-to-gasoline process: Topsøe integrated gasoline synthesis (TIGAS): Cooled, boiling-water MeOH/DME reactor and parallel adiabatic gasoline reactors.

Ironically, shortly after the MTG plant in New Zealand was put into operation, crude oil prices plummeted to levels between $ 10 and $ 20/bbl and remained low for more than a decade. Eventually, in the mid-nineties, the MTG part was shut down and the plant switched to methanol production. Following the period of low oil prices in the late eighties and through the nineties, the pick-up of oil prices during the last decade have spurred renewed interest in synfuels, and several projects in China and the USA have been announced. In 2009, a 100 kilotonne per year (kt/y) MTG

demonstration plant in Shanxi province, China, was brought on-stream. Other versions of the MTG process are currently in the demonstration phase, comprising the STF process (syngas-to-fuels; via methanol) developed by CAC Chemnitz (Germany), and a Chinese MTG process developed by Shanxi Coal Institute (China). A green version of the TIGAS process, based on biomass gasification, has been announced for demonstration in the USA.[5]

1.1.2. Mobil Olefin to Gasoline and Distillate (MOGD) Process

The selectivity to light olefins, which are intermediates in the MTG process, increases significantly at low pressure (kinetic effect) and high temperature (partly thermodynamic effect). These conditions were also realized in a fluid-bed pilot plant to produce a primary product of light olefins, gasoline being the secondary product. The concept was extended to make a combined gasoline/diesel product by subsequent oligomerization of the light olefins, and a demonstration was carried out at one of Mobil's refineries.[6] An outline of the MOGD process is shown in Figure 3.

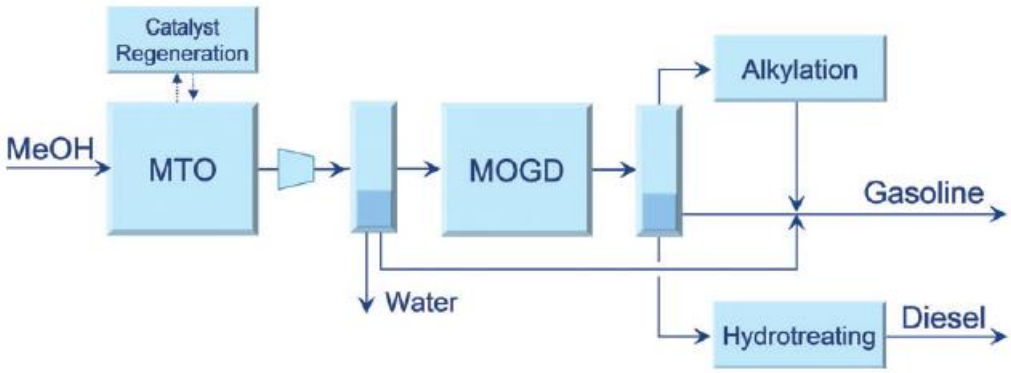

Figure 3. Mobil olefins to gasoline and distillate process (MOGD): Fluidized-bed MTO reactor (H-ZSM-5) with continuous regeneration and parallel fixed-bed reactors for gasoline and diesel synthesis.

1.1.3. Methanol to Olefins (MTO Process)

The selectivity towards light olefins was significantly improved by the discovery of H-SAPO-34 by researchers at Union Carbide (now UOP). Through its chabazite (CHA) structure of large cavities connected by 8-rings, selectivity to light olefins (ethene/propene) may exceed 80 % and conditions may be tuned to make propene the favored product. However, as opposed to H-ZSM-5, coking of H-SAPO-34 is rapid, requiring frequent regeneration. In the nineties UOP and Norsk Hydro (now INEOS) developed the H-SAPO-34 based MTO process, applying a low-pressure fluidized-bed reactor design to enable efficient temperature control and continuous regeneration.[7] Further improvement of ethene/propene selectivity was achieved by combining the UOP/INEOS MTO process with an olefin cracking process (OCP) developed jointly by Total Petrochemicals and UOP (Figure 4).[8] In 2009 a semi-commercial demonstration unit in Feluy, Belgium, processing up to 10 tonnes per day of methanol feed was brought on-stream, and in 2011 the construction of a 295 kt/y plant in Nanjing, China was announced.

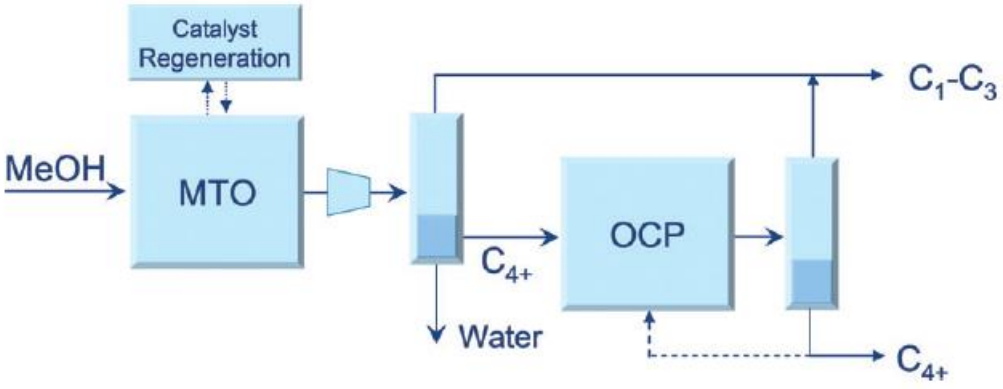

Figure 4. INEOS MTO methanol-to-olefins (MTO) fluidized-bed process (SAPO-34) combined with UOP/Total OCP olefin cracking process.

H-SAPO-34 is also the core catalyst in a similar process developed by researchers at Dalian Institute of Chemical Physics.9 The process, DMTO, also applies a fluidized-bed process, but includes recycle of C_{4+} olefins to maximize ethene and propene productivity. In 2010, a 600 kt/y (ethene+propene) plant was started in Baotou, China.

In parallel to the H-SAPO-34 development track followed by UOP/Hydro and DICP, Lurgi pursued the H-ZSM-5 route (using highly siliceous H-ZSM-5) with particular focus on maximizing propene yields. This, eventually, became the methanol-to-propylene (MTP) process where undesired products, such as primary olefins, ethene, and butenes, are simply recycled to the conversion step (see block diagram in Figure 5).10 The process design consists of parallel fixed-bed quench reactors, enabling intermittent regeneration, with feed injection between beds to control temperature. Recycling C_2 and C_{4+} olefins provide a heat sink for the exothermic reaction. Additional recycling of process condensate water acts as diluting agent and increases the selectivity to olefins. Synthesis pressure is close to atmospheric and temperatures are about 460–480 °C. The first plant was started up in China in 2010 with an annual capacity close to 500 kt/y of propene, with gasoline (185 kt/y) being the major by-product.

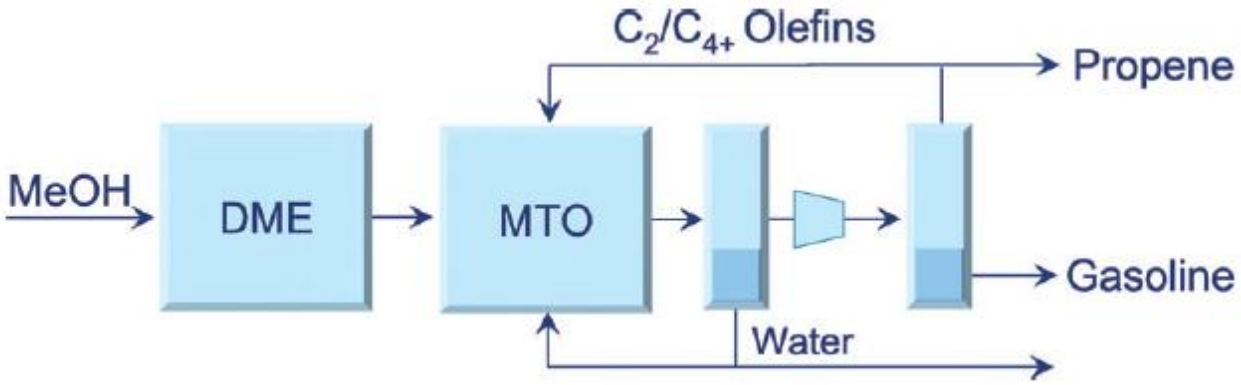

Figure 5. Lurgi MTP process: Adibatic dehydration reactor for DME synthesis and parallel adiabatic reactors with interstage feed (quench) addition and recycle of process condensate and C_2 and C_{4+} olefins.

2. Description of the Catalyst Structure

Despite the fact that H-SAPO-34 and H-ZSM-5 are the only two zeolites used in industrial MTH processes, a comprehensive screening on a large variety of materials characterized by different topologies (channels/cavity networks and dimensions; window openings giving access to internal cavities), compositions (number and distribution of acidic sites, defects), and morphologies (crystal dimensions, micro- and mesoporosity) has been performed over the last four decades. A selection of representative materials is discussed below. A list of these materials, including properties that we believe are important for their behavior in the MTH reaction, is shown in Table 1. For a more detailed description of each topology, we recommend the International Zeolite Association (IZA) database of zeolite structures, which contains all approved zeolite topologies.[11]

Shape selectivity is a key to the success of zeolite catalysis. Product selectivity can be explained well in terms of the dimensions of the windows restricting the access to the internal channel system. The simplest classification of channel dimension is by the number of T atoms forming the window, typically 12-, 10-, and 8-ring windows (with openings of 7, 5.5, and 4 Å, respectively). Larger organic intermediates and their interaction with the host structure form the active site (Section 3.2). The space requirements for these intermediates are often larger than the window dimensions and they will be trapped inside the cavities. The shape of the internal space is therefore important but cannot easily be described by numbers. Figure 6 compares the two most-studied topologies, MFI and CHA. These structures represent extremes; in MFI, the essential parameter is the space defined by channel intersections, while CHA consists of regular cavities connected by narrow windows. The TON structure represents another extreme, that is, a 1D topology without cavities and with 10-ring channels. This topology is shown in Figure 7. The effect of the various topologies on product selectivity are significant and are dealt with in Section 4.2.

Table 1. Topologies and materials discussed herein.

Topology	Material	Channel structure	Composition
BEA	beta	3D, 12-ring	Si/Al = 8–25
AFI	SAPO-5	1D, 12-ring	Al(50)P(34)Si(16)
MFI	ZSM-5	3D, 10-ring	Si/Al = 10–∞
MEL	ZSM-11	3D, 10-ring	Si/Al = 10–∞
TUN	TNU-9	3D, 10-ring	Si/Al = 20
IMF	IM-5	3D, 10-ring	Si/Al = 9–16
FER	ZSM-35	2D, 10-ring	Si/Al = 5–∞
TON	ZSM-22	1D, 10-ring	Si/Al = 30
MTT	ZSM-23	1D, 10-ring	Si/Al = 23
CHA	H-SAPO-34	3D, 8-ring	Al(50)P(30–45)Si(20–5)
	SSZ-13		Si/Al = 12
ERI	UZM-12	3D, 8-ring	Si/Al = 6
LTA	UZM-9	3D, 8-ring	Si/Al = 3.5–6
UFI	UZM-5	2D, 8-ring	Si/Al = 5–12
RTH	RUB-13	2D, 8-ring[a]	Si/Al = 90

[a] Effectively 1D owing to elliptical windows in the [001] direction.

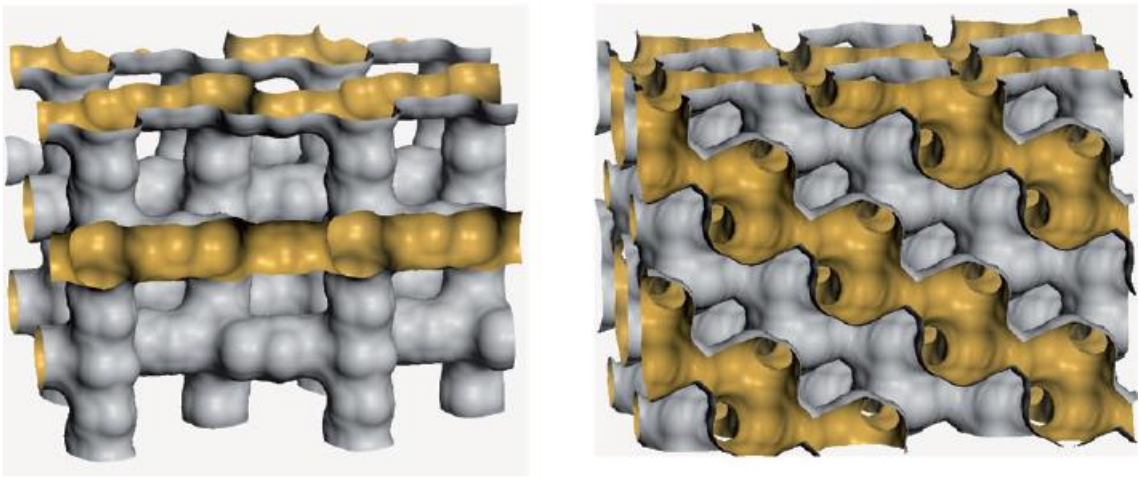

Figure 6. Shape and connection of the internal surface to the two zeolites that are in industrial use: H-ZSM-5 (left) and H-SAPO-34 (right). Both materials have a three-dimensional channel structure, but the shape is very different. The surface in H-ZSM-5 is best described as interconnected tubes, while H-SAPO-34 has larger cavities with narrow connections.

All materials of interest show medium-high Brønsted acidity given by the particular distribution of hydroxy groups (recognized to be one of the features responsible of catalysts performances both in terms of activity and lifetime). The need of knowledge about hydroxy group accessibility and acidity has encouraged an extensive use of IR spectroscopy conducted in controlled atmosphere and in combination with in situ studies with probe molecules.[12–18] In aluminosilicates, hydroxy groups generally absorb in the range of 3800–3600 cm^{-1}, depending on their acidities and local environment. Figure 8 a shows a collection of IR spectra obtained on a selection of zeolitic materials activated in high vacuum at 500 °C. All materials show a main band with a maximum at 3745 cm^{-1} and a multicomponent tail at lower frequencies, extending to 3700 cm^{-1} owing to the ν(OH) stretching mode of free or very weakly perturbed silanol groups on external surfaces and on internal nanocavities generated by silicon atom vacancies.

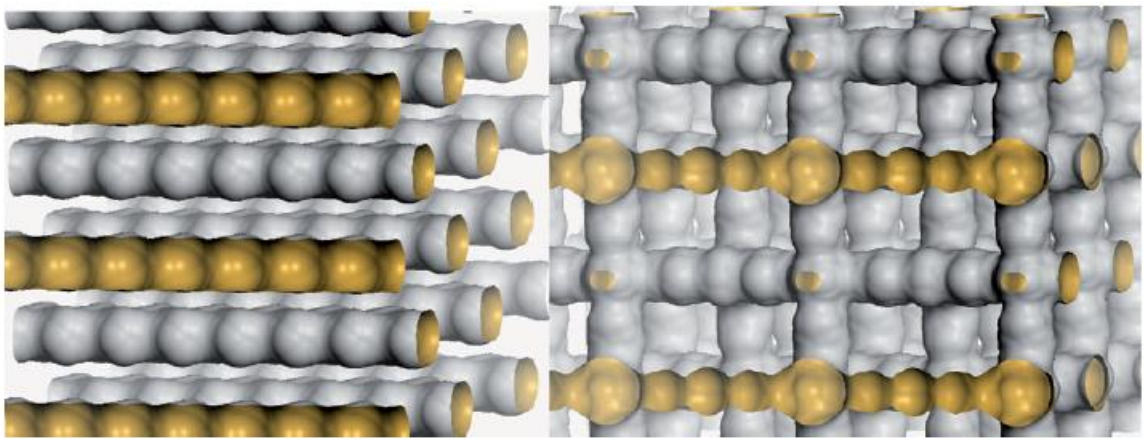

Figure 7. Comparison of the inner surface in the structures of H-ZSM-22 (left) and H-ZSM-5 (right). Both structures have 10-ring channels, but the intersections between orthogonal channels in H-ZSM-5 create a slightly larger volume.

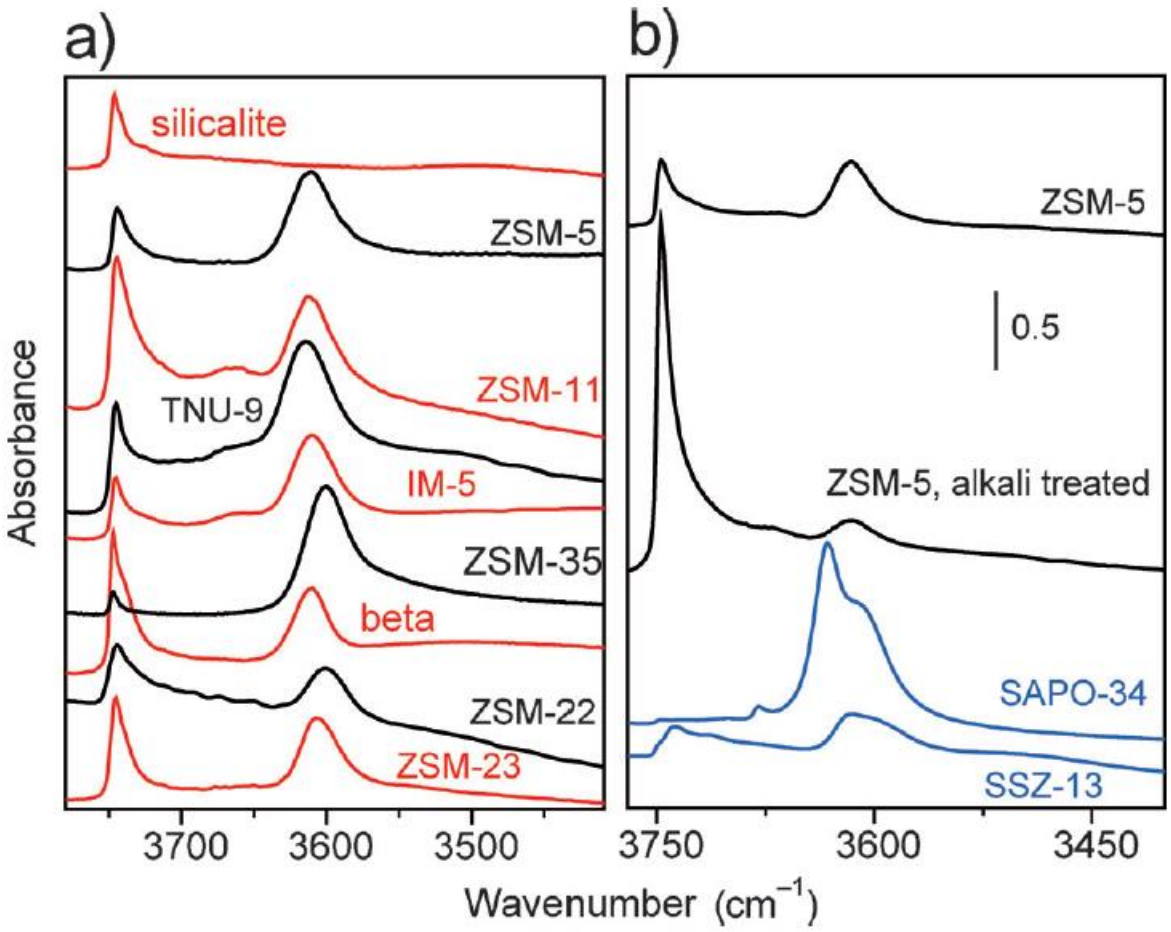

Figure 8. IR spectra of activated zeolites. a) From top to bottom: silicalite, H-ZSM-5, H-ZSM-11, H-TNU-9, H-IM-5, H-ZSM-35, H-Beta, H-ZSM-22 and H-ZSM-23. b) From top to bottom: H-ZSM-5, alkali-treated H-ZSM-5, H-SAPO-34, H-SSZ-13.

Recently, the relevance of these species with respect to catalyst deactivation rate has been pointed out (Section 6.1).[19–21] The second major component of the IR spectra of acidic zeolites is a band centered in the 3616–3605 cm^{-1} range. This band is attributed to the ν(OH) mode of the Si(OH)Al Brønsted sites. This is the typical stretching mode of extra-framework H^+ balancing the negative framework charge and its intensity is mostly associated with the Al content inside the zeolitic framework. Only few zeolites show multiplets owing to distinguishable acidic hydroxy groups, as shortly described below. Minor features are the band at 3665 cm^{-1}, which is due to partially extra-framework Al species, and broad bands extending below 3500 cm^{-1} associated to interacting silanol groups, which are due to internal defects. These species are mostly present in materials with low Al content and with intrinsic defectivity, such as beta zeolite, constituted by two polymorphs.[14]

As anticipated before, variable-temperature and -pressure IR spectroscopy measurements of zeolites interacting with molecular probes allow site accessibility and acidic strength to be investigated. In this respect, CO adsorption at −196 °C (liquid nitrogen) has been the most used approach, showing that the acid strength of all these materials (apart from silicalite, which does not contain any strong Brønsted sites) is very similar.[18]

Significant changes in hydroxy group characteristics are observed in samples on which post synthesis desilication treatments occurred,[19, 22] or in case of materials with the same framework

topology but with different compositions, such as H-SAPO-34 and H-SSZ-13.[15, 17] Comparison of the IR spectra of a standard H-ZSM-5 and the alkali treated counterpart (Figure 8 b) shows the decrease of the band that is due to strong Brønsted sites (3612 cm^{-1}), the increase of the peak ascribed to the free external silanol groups (3745 cm^{-1}), and the decrease of the component at 3726 cm^{-1} associated with isolated internal silanol groups.

Improved catalytic performances of desilicated materials encouraged spectroscopic combined studies (mainly IR and NMR) devoted to the characterization of these materials with respect to hydroxy group distribution and catalytic behavior.[20–22] IR spectra of H-SAPO-34 and H-SSZ-13 are different in many aspects, as evidenced by the comparison of the two spectra in Figure 8 b. H-SAPO-34 is characterized by a very low concentration of external hydroxy groups (Al—OH, P—OH, and Si—OH), while H-SSZ-13 shows an abundant variety of free silanol groups, as testified by a complex band extending from 3750 to 3700 cm^{-1}. Moving to the features associated to the strong Brønsted sites, both materials show clear doublets (H-SAPO-34: 3627 cm^{-1}, 3603 cm^{-1}; H-SSZ-13: 3616 cm^{-1}, 3584 cm^{-1}); both doublets are accessible to probe molecules. Significantly different shifts are observed for H-SAPO-34 and H-SSZ-13 upon interaction with CO, owing to their different acid strength ($\Delta\nu_{OH}$=−270 and −314 cm^{-1}, respectively).[23] However, high- and low-frequency bands from each sample give rise to a single red-shifted band upon interaction with CO. Conversely, when the probe molecule is H_2 adsorbed at 15 K, two maxima are observed for each sample, confirming the high potential of this experimental approach, which is also very sensitive in the detection of extra-framework Al sites.[13, 15, 17]

3. Reaction Mechanisms

Mechanistic studies have been at the core of MTH research for more than 30 years. Several reviews that extensively cover early research on this subject can be found in the literature,[24–27] but a brief introductory account will be given also herein.

Many techniques can infer information about the mechanism of heterogeneously catalyzed reactions. With respect to MTH, a primary challenge is to obtain simultaneous information about the gas-phase products and the reaction intermediates which to varying degrees are confined within the pores or cavities of the catalyst.

From a practical point of view, accurate overall kinetic data are in principle fairly straightforward to measure, requiring basic chromatographic methods and a well-defined reactor setup. However, as we shall see (Section 3.2), the translation of the kinetic phenomena observed in the MTH reaction into mechanistic insights requires sophisticated analysis. In general, measurements of rates and activation energies of individual reaction steps are indispensable to discriminate among pathways. However, due to the complex MTH reaction network, this approach requires particular attention with respect to experimental design.

Isotopic labeling is a powerful approach to elucidate reaction mechanisms, and this is indeed the situation for the MTH reaction. Two distinct procedures have been particularly successful. The co-reaction of [^{13}C]methanol with various unlabeled hydrocarbon species has been widely employed to investigate their reactivity and potential role as intermediates. Transient studies, relying on the abrupt switch from ordinary [^{12}C]methanol to [^{13}C]methanol have also provided insight on reactive intermediates versus spectator species and information concerning primary and secondary product formation without disrupting the reaction system by introducing reactants other than methanol. H/D exchange reactions have occasionally also been studied, but to a lesser extent.[28, 29]

As mentioned above, owing to the porous nature of the zeotype catalysts and the bulky nature of many suggested reaction intermediates, careful studies of these species are required and have been achieved by a procedure introduced by Guisnet and co-workers.[30] By employing thermal quenching of the reaction followed by dissolution of the encapsulating catalyst framework in

hydrofluoric acid, these species are liberated and available to analysis (often by GC-MS) after extraction in an organic solvent. This method has allowed exact structural identification of hydrocarbons present within the catalyst voids during the MTH reaction, and when combined with isotopic labeling, information on reactivity might be obtained.

Spectroscopy has been employed to identify the various surface sites on the catalysts prior to reaction (Section 2) and the interaction between these sites and methanol and intermediates/products. Solid-state vibrational spectroscopy (FTIR and Raman) and solid-state NMR spectroscopy have proven to be particularly useful, whereas diffuse-reflectance UV/Vis spectroscopy has been employed mostly to investigate species leading to catalyst deactivation. A clear advantage of spectroscopic techniques compared to the dissolution/extraction method described above is the possibility to perform in situ analyses.

Finally, computational methods have matured substantially, and it is now possible in favorable cases to predict kinetic parameters and rates of reaction with near chemical accuracy.[31, 32] Such methods may also facilitate the interpretation of spectroscopic results. A clear advantage compared to experimental methods is the possibility to selectively choose which reaction steps or properties to determine without the interference of competing reactions or the presence of several species at once.

3.1. Setting the Scene: Developments Leading to the Hydrocarbon-Pool Mechanism

The mechanism of the MTH reaction has been the subject of vast amounts of research. Initial research focused on possible routes for the formation of initial C—C bonds from C_1 units, that is, methanol or dimethyl ether. More than 20 possible mechanisms have been proposed, encompassing a variety of reactive intermediates. Among them are oxonium ylides,[33–35] carbocations,[36, 37] carbenes,[38–40] and free radicals.[41, 42] However, little experimental evidence in favor of any of these proposals has appeared,[27, 43] and theoretical methods most often yield prohibitively high energy barriers.[44–48]

The issue of C—C bond formation directly from methanol was addressed by Song et al.[49] When using reactants, carrier gases, and catalysts extensively purified from C—C bond-containing impurities, the initial rate of methanol conversion was reduced by orders of magnitude. Thus, it seems clear that direct formation of C—C bonds from C_1 units is of no importance during steady-state conversion, and it is unlikely that direct conversion is important during an induction period with normal feedstocks. Any such reactions are probably overshadowed by the co-reaction of methanol with hydrocarbon impurities from various sources. Thus, possible routes of direct C—C bond formation are most likely of little practical importance, but remain an intriguing question.[50–55]

Some characteristics of the MTH reaction were described quite early. The MTH reaction is autocatalytic,[1, 36, 56] in the sense that the presence of small amounts of products leads to an enhanced rate of conversion, until steady state is eventually reached. Linked to this, an induction period is often observed,[36, 51, 57, 58] meaning that the level of methanol conversion increases with time during the initial stages of the reaction. In 1986, Dessau, from Mobil's laboratories, stated that "*asking where the first olefin comes from is analogous to asking where the first peroxide comes from in an autooxidation reaction*".[59] Based on this, Dessau and co-workers proposed the indirect reaction model based on consecutive methylation and cracking:[59, 60] After the necessary alkenes are formed during the induction period, all ethene and higher alkenes are produced by repeated methylations, oligomerization, and cracking. Aromatics and alkanes are end products of cyclization reactions and hydrogen transfers (aromatization).[24]

An alternative to this alkene-based model exists, focusing on aromatics and other unsaturated cyclic species as the propagator of an indirect alkene formation route. The profound influence of aromatics on the MTH reaction was first noted by Mole and co-workers.[61, 62] It was observed that adding

small amounts of toluene or *p*-xylene resulted in an enhanced rate of methanol conversion; the effect was called aromatic co-catalysis.
Dahl and Kolboe later showed, using isotopic labeling, that both ethene and propene displayed little reactivity when co-reacted with methanol over H-SAPO-34.[63–65] Most of the products were formed exclusively from methanol, and the alkenes were basically inert under the reaction conditions investigated. However, later studies have shown that propene has a greater reactivity on H-ZSM-5 type catalysts.[66, 67] The low reactivity of the alkenes in H-SAPO-34 led Dahl and Kolboe to propose the hydrocarbon-pool mechanism, as shown in Figure 9. The hydrocarbon pool, with an initially specified overall stoichiometry $(CH_2)_n$, was said to represent an adsorbate which may have many characteristics in common with ordinary coke and might easily contain less hydrogen than indicated. The chemical structure of the pool was not further specified.[63–65]

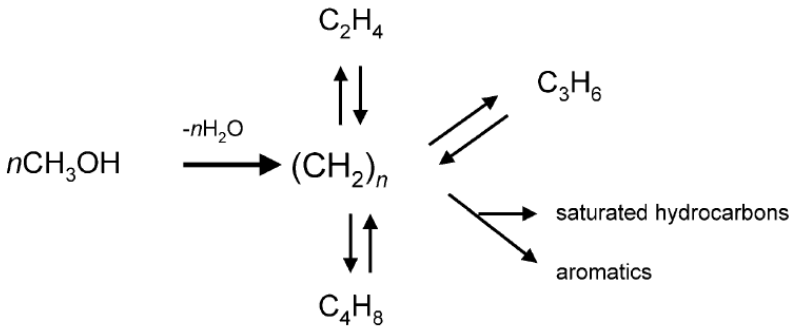

Figure 9. Depiction of the hydrocarbon-pool mechanism as originally proposed by Dahl and Kolboe. From Refs [63–65].

Methanol has been co-reacted with benzene or toluene, and it was concluded that an arene, or some arene derivative, is involved in forming a substantial part, or all, of the propene.[68] Arstad and Kolboe investigated the stability of species trapped inside the H-SAPO-34 cavities during methanol conversion, and their results further pointed towards methylbenzenes as key components of the hydrocarbon pool.[69, 70] Parallel studies by Haw and co-workers also identified methylbenzenes as the organic reaction centers for methanol to hydrocarbon catalysis on H-SAPO-34 catalysts,[71–75] in accord with the reports from Arstad and Kolboe mentioned above.[69, 70] These studies were extended to include zeolite H-beta, and the reactivity of several polymethylbenzenes and butylbenzene isomers was investigated.[76, 77] Haw and co-workers also investigated the MTH chemistry on an H-ZSM-5 catalyst using solid-state NMR spectroscopy, and it was found that methylated cyclopentenyl cations might also function as reaction centers for alkene formation.[78–81] Bjørgen et al. investigated the reactivity of polymethylbenzenes over the large pore zeolite H-beta, and the heptamethylbenzenium cation was identified as a key intermediate.[82–85]

It seems clear that methylbenzenes and their protonated counterparts (or other related cyclic species) are central reaction intermediates for alkene formation in the MTH reaction. How then are the alkenes formed from such species? Two distinct hypotheses exist, namely the so-called paring and side-chain methylation models. The paring model shown in Figure 10 (left) was adapted from a similar mechanism proposed by Sullivan et al. in 1961 to rationalize the product distribution observed when hexamethylbenzene was reacted over a bifunctional nickel sulfide on silica–alumina catalyst or over the purely acidic silica–alumina support.[86]

In this context, the word paring refers to an imagined process where methyl groups are shaved off the methylbenzene as alkenes. Direct evidence of paring-type reactions was obtained in investigations of the unimolecular decomposition of protonated methylbenzenes using mass

spectrometry.[87, 88] Alternatively, the side chain methylation Scheme shown in Figure 10 (right) for propene formation was proposed by Mole and co-workers[61, 62] and later refined by Haw and co-workers.[76, 77] Ethene and isobutene formation may proceed analogously, invoking only one or three deprotonation/methylation steps, respectively. Additional spectroscopic evidence in favor of side-chain methylation on H-ZSM-5 catalysts has been obtained by Hunger and co-workers,[89] who also have employed in situ NMR to examine several aspects of MTH chemistry.[90–94] It should also be noted that a lower homologue of the heptamethylbenzenium ion, the *gem*-dimethyl isomer of the pentamethylbenzenium ion, has been observed in zeolite H-ZSM-5.[95]

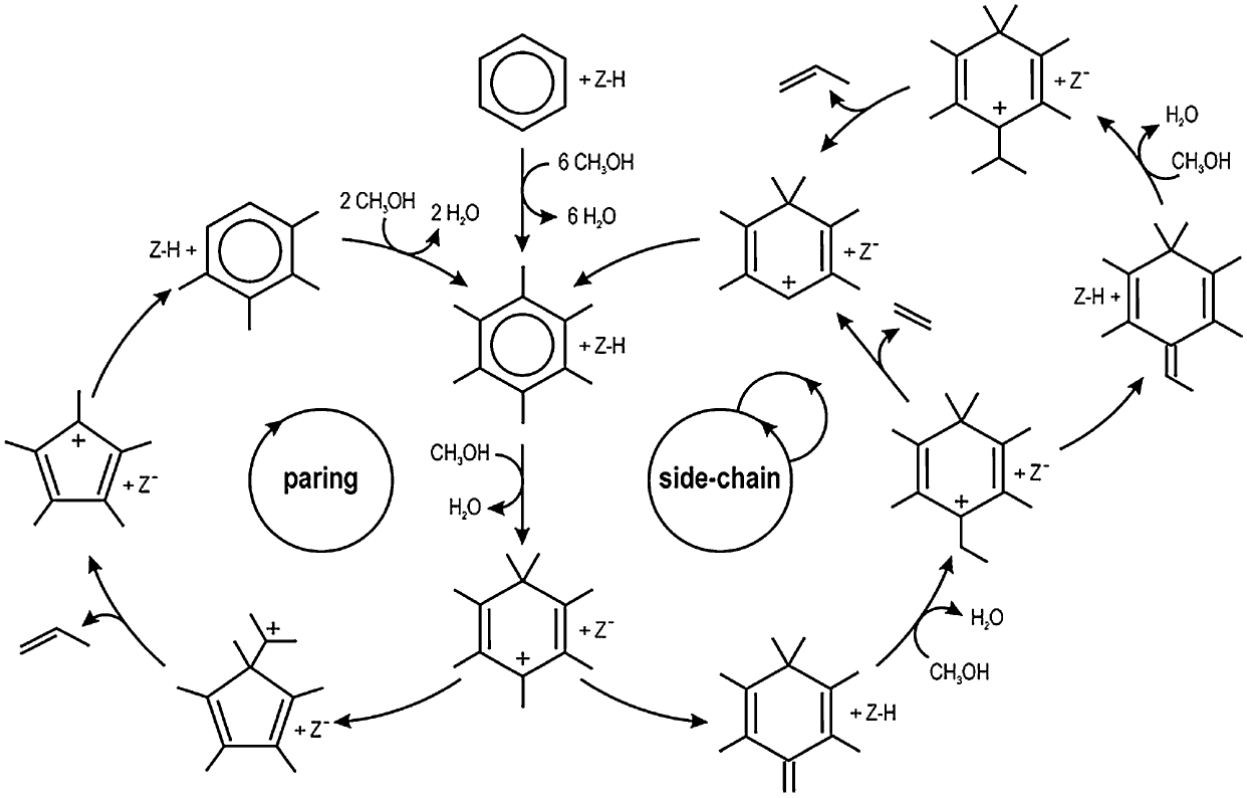

Figure 10. Representation of the paring and side-chain reaction concepts in MTH catalysis. From Ref. [120].

3.2. Recent Developments in the Mechanistic Understanding of the MTH Reaction

3.2.1. Kinetics and Autocatalysis

In the late 70s and early 80s, the autocatalytic mechanism for the H-ZSM-5-catalyzed transformation of methanol to hydrocarbons was recognized.[36, 56] The autocatalytic effect at 350 °C and atmospheric pressure, a typical process temperature, is illustrated in Figure 11. The upper panel shows the variations in hydrocarbon yield and the corresponding flow through the reactor during three repeated cycles in which the flow was gradually decreased and increased with time. Clearly, an increase of the flow from 40 to above 100 N mL min^{-1} results in a decrease in hydrocarbon yield from nearly 100 % to 0 %; when the flow is lowered again, the hydrocarbon yield increases steeply to 100 % again. When this cycle is repeated, the same hydrocarbon yields are obtained. The lower panel shows these hydrocarbon yields as a function of the catalyst weight to

flow ratio W/F, which can be regarded as the contact time. This yields an S-shaped curve for the hydrocarbon yield, which is characteristic for autocatalytic reactions.

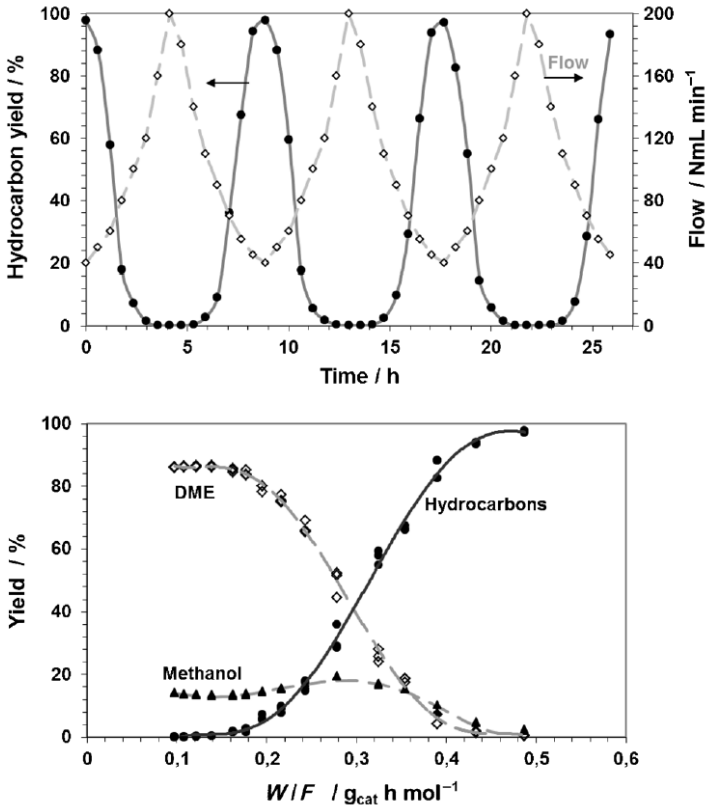

Figure 11. Top: Measured hydrocarbon yields in repeated cycles in which the flow was varied on a H-ZSM-5 catalyst at 350 °C and atmospheric pressure. The reactor consisted of a quartz U-tube with 4 mm inner diameter, filled with 52.2 mg of catalyst (150–300 µm sieve fraction). The exit-gas composition was determined by GC. Bottom: Measured hydrocarbon yield, also shown on the top plot, and the carbon-atom based concentrations of methanol and DME as a function of the contact time *W*/*F* (g_{cat} h mol^{-1}).

The S-shaped curve results from a reaction in which the hydrocarbon formation is initiated with a slow formation of hydrocarbon products, and then accelerated by a much faster reaction of methanol with these hydrocarbon products.[36, 56] The simplest reaction consists of an initiation and an auto-accelerating step [Equation (1)]:

$$\begin{aligned} &M \xrightarrow{k_1} P \\ &M + P \xrightarrow{k_2} P \end{aligned} \qquad (1)$$

where M and P correspond to methanol and products, respectively, and k_1 and k_2 are the rate constants for the reaction. The methanol concentration is then given by Equation (2):

$$\frac{dM}{d\tau} = -k_1 M - k_2 MP \qquad (2)$$

where M is the (carbon-atom-based) methanol concentration, P the concentration of the hydrocarbon products causing the acceleration of the reaction, and τ is the contact time. Introducing the conversion and using the relationship $M+P=M_0+P_0$ and the starting condition $M=M_0$ at $\tau=0$, the conversion can be written as:((3))

$$X = 1 - \frac{k_1 + k_2(M_0 + P_0)}{(k_1 + k_2 P_0)\exp(k_1 + k_2(M_0 + P_0)\tau) + k_2 M_0} \qquad (3)$$

Equation (3) can be rewritten to the expression derived by Ono for a first-order reaction, for $P_0=0$, and substitution of $\alpha=k_1/(k_2M_0)$.[36] If $k_1 \ll k_2$, Equation (3) results in a S-shaped curve for the conversion.

The autocatalytic process was originally attributed to a reaction between methanol and olefins; which is much faster than the formation of the first hydrocarbon fragments.[36, 56] The explanation of Espinoza[96] that a critical amount of DME is needed for the reaction to proceed can be ruled out, because the measured methanol and DME concentrations in Figure 11 indicate that the methanol/DME equilibrium is established at the lower contact times, and thus the critical amount of DME must be present under these conditions. Later, the hydrocarbon-pool mechanism was developed, which describes the hydrocarbon formation from methanol entirely by reactions of methanol with hydrocarbon fragments, predominantly olefins and aromatics (see below). Numerous other mechanisms have been proposed to form hydrocarbons from methanol; in many of them, a C—C bond is created by methylation of C_1 fragments or DME.[79, 97, 98] In this case, k_1 in Equation (3) is small and $P_0=0$. Another proposed reaction path to create a C—C bond is by a reaction between methane and protonated formaldehyde.[99] Nevertheless, it is generally accepted today that the reactions between methanol and the hydrocarbon pool is the most important pathway for the conversion of methanol on zeolites.[24]

The mechanisms entirely based on reactions of methanol with hydrocarbons and the mechanisms based on a C—C bond formation lead to very similar expressions for the conversion according to Equation (3). Consequently, the observed behavior of the conversion with contact time can be equally well explained by both scenarios. However, as described in Section 3.2.2, a feasible pathway for a direct C—C coupling reaction has not been identified yet, and the scenario based on reactions of methanol exclusively on hydrocarbon molecules seems more probable.

The fact that the observed hydrocarbon yield keeps following the same S-shaped curve when the flow cycles are repeated (see Figure 11) shows that there is a critical contact time below which hydrocarbon formation does not take place[96] and that at 350 °C the induction period is short. Consequently, the hydrocarbon species responsible for the autocatalytic effect disappear upon increasing the flow, and must be formed again when the flow is lowered: If the total amount of hydrocarbons remained constant, the conversion would decrease towards the origin of the plot, and not repeatedly show the S curves. Schulz et al. has shown that below 300 °C, the hydrocarbon formation increases with time, corresponding to a slower build-up of the hydrocarbons at these temperatures leading to an induction period.[100]

Adding hydrocarbons, such as propanol, propene, or aromatics, to the methanol feed accelerates the formation of hydrocarbons. This corresponds to a case where P_0 in Equation (3) is increased, and the conversion increases faster with the contact time. If the concentration of added hydrocarbons in

the feed is not significantly larger than the methanol concentration, the autocatalytic effect is still noticeable; only if P_0 becomes much larger than the methanol concentration, the reaction becomes pseudo first order. The reactivity for different hydrocarbons, however, is not the same. The rate of methylation of the olefins on H-ZSM-5 increases with the chain length of the olefin; therefore, the methylation of ethene is slower by at least an order of magnitude.[31, 124] This implies that the self-acceleration effect of the MTH reaction is more pronounced for propene and the higher olefins than for ethene.

3.2.2. Introduction of the Dual-Cycle Concept: Structure–Selectivity Relationships

Until 2006, the major part of the fundamental understanding of the hydrocarbon-pool mechanism was compiled for the relatively spacious H-SAPO-34 and H-beta catalysts. For these two catalysts, the main catalytic engines of the hydrocarbon pool was concluded to be the higher methylated benzenes or their protonated counterparts. For H-beta, the heptamethylbenzenium cation displays the greatest reactivity for alkene formation, whereas hexamethylbenzene behaves similarly in H-SAPO-34 (Figure 10). Clearly, the detailed reaction mechanism might be expected to vary with pore architecture, and detailed mechanistic reexamination of H-ZSM-5 was undertaken in 2006.[101, 102] Using the dissolution/extraction procedure described above, it was shown that for H-ZSM-5, the higher methylbenzenes up to hexamethylbenzene are present in the H-ZSM-5 pores. However, based on transient $^{12}C/^{13}C$ switching experiments, the higher methylbenzenes were shown to be virtually inert, in stark contrast to the observations previously made for H-SAPO-34[69–75] and H-beta.[76–85] These key findings were based on the data shown in Figure 12,[101, 102] which displays the percentage of ^{13}C originating from fresh methanol in the gas-phase products (left) and in the hydrocarbons retained within the zeolite pores (right) as a function of reaction time after the feed switch. In this experiment, it is possible to distinguish active from inactive species in the working catalyst, as more reactive species will show faster ^{13}C incorporation, giving rise to higher total ^{13}C contents in the compounds. Clearly, the rate of ^{13}C incorporation in the methylbenzenes decreases with increasing degree of methyl substitution, which is indicative of low reactivity. A second interesting feature is borne out in Figure 12. Based on the very similar total ^{13}C contents and development with time, a mechanistic link between ethene and the xylenes and/or trimethylbenzenes could be established. It was concluded that the aromatics-based hydrocarbon-pool mechanism was the predominant source of ethene over H-ZSM-5. The significantly higher rate of ^{13}C incorporation in the C_{3+} alkenes compared to ethene and the most reactive methylbenzenes showed that propene and higher alkenes to a considerable extent are formed from alkene methylations and interconversions, such as cracking reactions.[101, 102] The major distinction between this methylation/cracking cycle compared to the homologation already proposed by Dessau[59, 60] is that ethene is not included. This is reasonable, as it has been demonstrated that ethene is a very unlikely product in the cracking of higher alkenes.[103] Thus, it was suggested that two mechanistic cycles run simultaneously during the MTH reaction over H-ZSM-5: ethene (and propene[104]) formation from the lower methylbenzenes followed by re-methylation, and methylation/cracking involving only the C_{3+} alkenes (not ethene). The idea was referred to as the dual-cycle concept and is summarized in Figure 13.[101, 102, 105] This constitutes a refinement of the hydrocarbon-pool mechanism as proposed by Dahl and Kolboe.[63–65] The C_{3+} alkenes involved in the alkene methylation/cracking cycle bear great resemblance to the autocatalytic species P in Equation (1) above, at least for H-ZSM-5, which has a pore architecture that allows these alkenes to be released into the gas phase. The main distinction between the general term autocatalytic mechanism and the hydrocarbon-pool mechanism therefore appears to be the diffusion restrictions associated with the hydrocarbon-pool species. As shown by the examples given in this Review, no clear cut-off can be made since diffusion restrictions depend on catalyst topology as well as reaction

conditions. It is thus convenient to stick to the more generalized definition of the term hydrocarbon-pool species originally proposed by Dahl and Kolboe, comprising both alkenes and multiply methylated benzenes/benzenium ions, including the heptamethylbenzenium cation, which is the terminal methylation product. Bicyclic species such as methylated naphthalenes might undergo similar reactions leading to alkene formation, but such compounds are known to be less reactive and thus of less relevance.[72, 83]

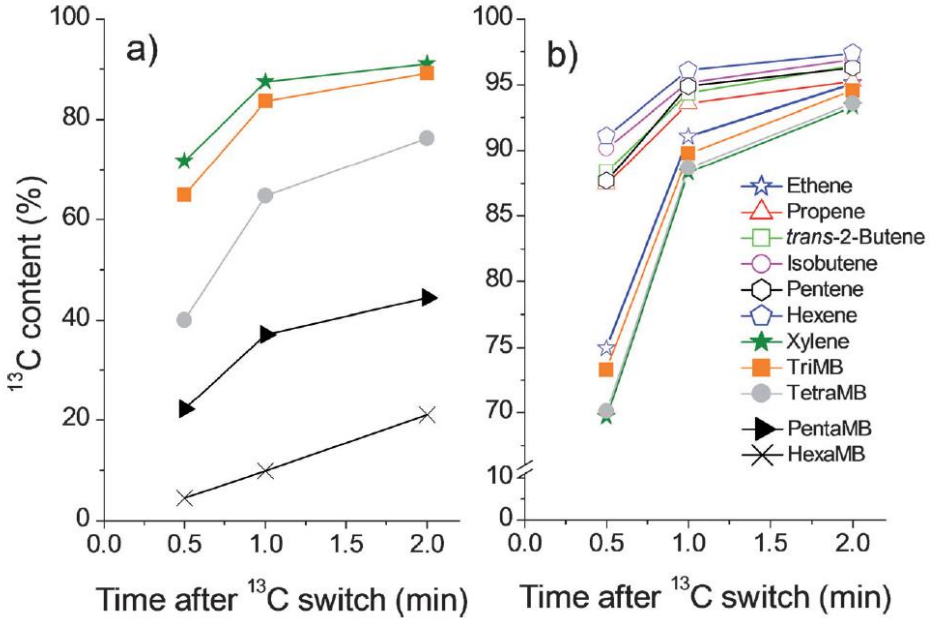

Figure 12. Transient $^{12}C/^{13}C$ methanol switch experiment carried out using H-ZSM-5 (Si/Al=140). Methanol (WHSV=7.0 g g^{-1} h^{-1}) was reacted from the gas phase in a fixed-bed reactor at 350 °C. ^{12}C methanol was fed for 18 min before switching to ^{13}C methanol and reacting further for a predetermined time. The time evolution of ^{13}C content in effluent (b) and retained material (a) was determined from GC-MS analyses performed 0.5, 1.0, and 2.0 min after $^{12}C/^{13}C$ methanol feed switch. Adapted from Ref. [101].

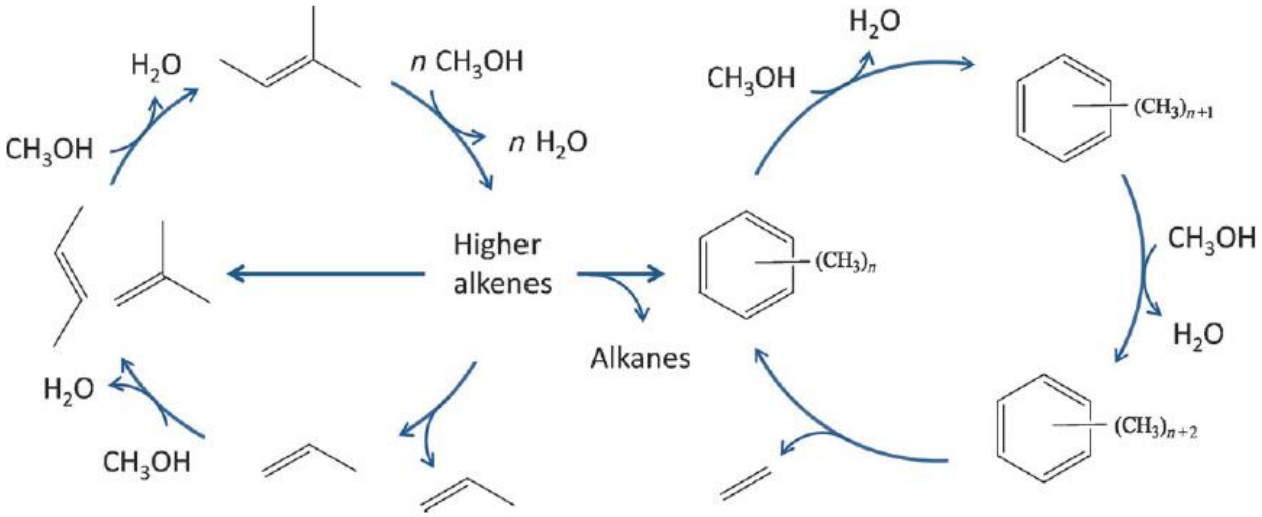

Figure 13. Suggested dual-cycle concept for the conversion of methanol over H-ZSM-5.

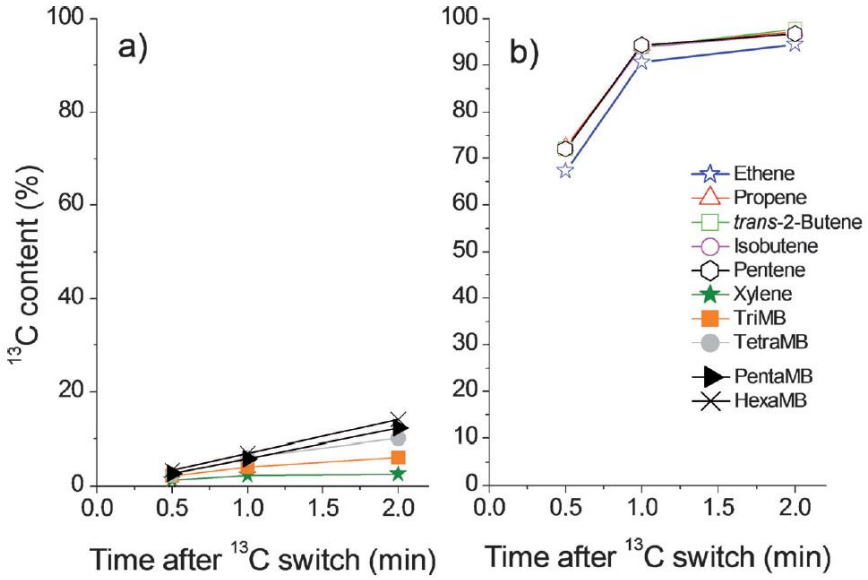

Figure 14. Transient $^{12}C/^{13}C$ methanol switch experiment carried out using H-ZSM-22 (Si/Al=30). Methanol (WHSV=2.0 g g^{-1} h^{-1}) was reacted from the gas phase in a fixed-bed reactor at 400 °C. ^{12}C methanol was fed for 18 min before switching to ^{13}C methanol and reacting further for a predetermined time. The time evolution of ^{13}C content in effluent (b) and retained material (a) was determined from GC-MS analyses performed 0.5, 1.0, and 2.0 min after $^{12}C/^{13}C$ methanol feed switch. Adapted from Ref. 107.

A highly interesting question regarding both mechanistic understanding and selectivity control was highlighted as the dual-cycle concept was introduced:101, 102 Can the two cycles of the dual-cycle mechanism operate completely independently or are they intertwined in some manner? It was argued that a completely independent operation cannot be the case for H-ZSM-5. Aromatics are constantly formed during the reaction through aromatization of higher alkenes formed in the alkene methylation/cracking cycle. This implies that the aromatics-based cycle cannot run independently over H-ZSM-5. However, by choosing a catalyst topology suppressing the aromatics-based cycle, it can be imagined that methanol can be converted solely according to the alkene methylation/cracking cycle, thus strongly reducing the yield of ethene.101, 102, 105 Understandably, manipulating the ethene production is of utmost importance for selectivity control in MTO/MTP applications. Based on the observed product distribution of the MTH reaction over H-Ferrierite, a similar notion was also presented by Haw et al.79 This possibility of achieving selectivity control based on fundamental insights was addressed in two recent publications where H-ZSM-22 was employed as catalyst.106, 107 Based on experiments carried out at very high feed rates leading to non-observable conversion, it had been suggested that the aromatics-based cycle might be suppressed in the H-ZSM-22 topology comprising unidirectional 10-ring channels without the additional space afforded by intersections.108, 109 However, in more recent experiments employing substantially lower feed rates, appreciable conversion and catalyst lifetime were observed also for H-ZSM-22.106 Moreover, a product mixture very rich in highly branched C_{5+} alkenes with negligible content of aromatics was found (see also Figure 15), which is indicative of extensive product formation by the alkene methylation/cracking cycle.106 Figure 14 shows the outcome of a $^{12}C/^{13}C$ methanol transient switching experiment carried out for H-ZSM-22 in a manner similar to that displayed for H-ZSM-5 in Figure 12. The total ^{13}C contents in both the gas-phase alkene products and the aromatic species retained within the pore system are displayed. Clearly, the retained aromatics display virtually no reactivity towards the fresh ^{13}C methanol, showing that these species are of little importance as reaction intermediates in H-ZSM-22. This, in turn, implies that product formation by the aromatics-based cycle is negligible. As expected,

considering the equilibrating nature of the alkene methylation/cracking cycle, the alkenes in the gas phase display practically identical rates of ^{13}C incorporation, including ethene, which is a very minor product (see below). Therefore, by careful considerations of the steric properties of the catalyst topology it was possible to suppress product formation by the aromatics-based cycle whilst leaving the C_{3+} alkene-based cycle operative.[107] These experiments pertaining to the MTH mechanism over H-ZSM-22 were later reproduced by Li et al.[110, 111]

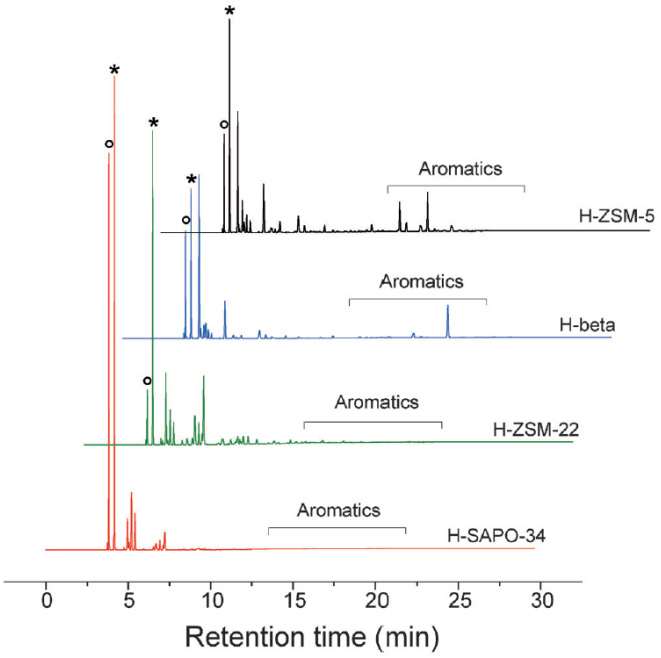

Figure 15. Chromatograms showing the MTH product distribution at 100 % conversion over different catalysts; H-ZSM-5 (Si/Al=50), H-beta (Si/Al=45), H-ZSM-22 (Si/Al=30), and H-SAPO-34 ((Al+P)/Si=11). WHSV=2 g g^{-1} h^{-1} and 400 °C. The ethene peaks are indicated by ○ and the propene by ⋆. From Ref. [107].

We are now at a position where we can rationalize many of the features observed in the product spectrum of different MTH catalysts. Figure 15 shows chromatogram traces of the products detected in the effluent during the MTH reaction at 400 °C over four catalysts having different topologies.[107] All of the catalysts have a reasonably similar and high density of acid sites (Si/Al 30–50) except H-SAPO-34, which has the typical density of acid sites corresponding to one site per cavity. Based on the comments above, the high propene/ethene ratio observed for H-ZSM-22 is a direct consequence of the very minor role of the aromatics-based cycle, which is the predominant source of ethene in MTH chemistry in this sterically restricted topology. For H-SAPO-34, the well-known MTO catalyst, ethene and propene are clearly dominant and the highest products are linear pentenes. This is due to the prominent product shape selectivity for this narrow-pore catalyst. Based on temperature-variation experiments, Barger suggested that equilibration of ethene and propene is established prior to diffusion out of the crystalline structure.[26] The dominating role of product shape selectivity in H-SAPO-34 was later confirmed by Hereijgers et al.[112] Thus, it is not straightforward to extract mechanistic information from the effluent composition of the diffusion-controlled H-SAPO-34 system. As seen in Figure 15, both H-ZSM-5 and H-beta produce significant amounts of both ethene and propene. The formation of sizable amounts of ethene over these two catalysts is ascribed to the significant contribution of the aromatics-based hydrocarbon-pool-type reaction mechanism. However, it may be noted that the propene/ethene ratio is significantly higher for H-beta compared to H-ZSM-5. This effect is even more pronounced in experiments carried out

at 350 °C, where the propene/ethene ratio obtained over H-beta is 21 compared to 3 for H-ZSM-5.[113] This result has been ascribed to the difference in the nature of the most active methylbenzene intermediates in these two catalyst systems. As mentioned above, it is the higher methylbenzenes that are intermediates in alkene formation in H-beta, whereas the lower methylbenzenes play the analogous role in H-ZSM-5. Haw and co-workers studied the alkene selectivities in the MTO reaction over H-SAPO-34, and concluded that the propene/ethene ratio is related to the average number of methyl groups on the benzene rings trapped in the cavities of the catalyst.[73] From correlations of ^{13}C NMR spectra of retained hydrocarbons to the propene/ethene ratio in effluent, it was suggested that propene is favored by methylbenzenes with four to six methyl groups, whereas ethene is predominantly formed from methylbenzenes with two or three methyl groups.[73] These findings were later supported by gas-phase experiments in which the unimolecular decomposition of polymethylated benzenium ions was studied by mass spectrometry.[87, 88] Armed with this insight, it is reasonable that the hydrocarbon-pool mechanism operating in H-ZSM-5, which is based on the lower methylbenzenes, yields predominantly ethene, whereas for H-beta, the higher homologues are active and propene is favored.[113] This shows how it is possible to establish links from a molecular-level mechanistic understanding and the actual product selectivity in the industrially relevant MTH reaction.

3.2.3. Computational Chemistry: Evaluation of Mechanisms for Alkene Formation

As mentioned above, computational chemistry is an indispensable tool to elucidate mechanistic details, and this is clearly also the case for the MTH reaction mechanism. Many reports deal with individual, or selections of a few, issues that are relevant for the overall MTH mechanism. Common examples are the adsorption geometries of methanol or dimethyl ether, the formation of dimethyl ether or surface-bound methoxy groups, possible routes for formation of C—C bonds from C_1 species, and various reaction steps, such as methylation, alkylation/dealkylation, and cracking reactions. However, the purpose of this section is not to give an exhaustive summary of the literature dealing with these singular issues, but rather to summarize the literature evaluating complete catalytic cycles for alkene formation. A central issue, which thus far has been investigated mostly theoretically, is to discriminate between the paring and side-chain methylation proposals for alkene formation from methylbenzenes (see Figure 10). It should be noted that comparisons of theoretical work is not always straightforward owing to differences in the computational approaches, the reactions selected for study, and the strategies employed to model the shape selectivity of the porous catalysts.

Initial theoretical work on the paring mechanism was carried out without accounting for the encapsulating nature of the zeolite at all, that is, by investigating the suggested intermediates as protonated species in the gas phase.[114–116] Pathways leading to the loss of ethene from protonated xylenes[114] and small alkenes from the heptamethylbenzenium ion[115] by ring contractions or expansions were found. Ring-expansion mechanisms for alkene formation involving seven-membered rings had not been considered previously (Figure 10). The plausibility of the side-chain methylation route via several *gem*-dimethylated benzenium ions was also supported theoretically, with similarly limited efforts to model the topological constraints of the catalyst.[117] However, although providing detailed structural insights, these initial gas-phase calculations did not allow confident discrimination based on energetic considerations owing to the incomplete description of the zeolite framework.

McCann et al. reported a complete catalytic cycle for supramolecular isobutene formation according to the paring route based on methylation of toluene followed by ring contraction of

methylbenzenium ions into cyclopentenyl cations.[118] An ONIOM ("our own *n*-layered integrated molecular orbital and molecular mechanics") approach based on a very large cluster was employed to take the H-ZSM-5 framework into account. The methylation of toluene to form protonated xylene was found to be the rate-determining step, with an activation energy of about 160 kJ mol^{-1}.[118, 119] Subsequently, the same researchers studied ethene formation by side-chain methylation in H-ZSM-5 using similar methods.[120] A route leading to ethene formation was found, but the activation energy for the final ethene loss was rate-limiting and always very high (ca. 200 kJ mol^{-1}). This result led to the conclusion that side-chain methylation was an unlikely route to ethene from methanol, and it was suggested that this might rather be a deactivating route leading to coke precursors.[120] In parallel, side-chain methylation was also investigated by Wang et al.[121, 122] They employed periodic DFT to account for the H-SAPO-34 framework. It was found that, starting from hexamethylbenzene, propene was the favored product over ethene, owing to a prohibitively high barrier for ethene formation. The rate-determining step in the propene formation was the second methylation of an exocyclic bond, with a barrier of about 210 kJ mol^{-1}.[121] Also, the calculations indicated that the most fully methyl-substituted methylbenzenes are not more reactive than those with fewer methyl groups, in apparent contrast to experimental reports.[69–71] For a side chain methylation catalytic cycle for propene formation based on trimethylbenzene in H-SAPO-34, the barrier of the rate determining methylation step was found to be about 180 kJ mol^{-1},[122] that is, about 30 kJ mol^{-1} lower than for the cycle based on hexamethylbenzene. Chan and Radom also considered ethene formation by side-chain methylation of xylene using an 8T cluster model and relying on high-level single-point calculations for accurate energies.[123] Methylation of xylene was found to be the most energy demanding step in the process, with a barrier of about 165 kJ mol^{-1}.[123] Notably, Wang et al.[121, 122] and Chan and Radom[123] identified a different rate-determining step in the side chain methylation route than McCann et al.[118] The reason for this discrepancy is unclear. Very recently, Lesthaeghe et al. provided a full theoretical cycle for both ethene and propene formation by the alkene methylation/cracking cycle over H-ZSM-5 based on the ONIOM approach mentioned above.[124] The barriers for alkene methylation and cracking into C_{3+} products were found to be low and of comparable height (60–80 kJ mol^{-1}), which is indicative of an efficient catalytic process. In agreement with the experimental reports, the barriers for ethene formation by cracking of higher alkenes, was found to be substantially higher (90–120 kJ mol^{-1}).[124]

The quantum-chemical investigations summarized above provide impressive detail to our understanding of the MTH reaction mechanism. Based on a study pertinent to H-ZSM-5, it appears that isobutene formation from methylbenzenes via the paring mechanism is plausible, as no prohibitive energetic bottlenecks were identified.[118] The alkene methylation/cracking cycle that forms part of the dual cycle concept is also predicted to run efficiently, with fairly low barriers throughout.[124] Moreover, the calculations confirm that ethene formation by alkene cracking is appreciably slower than propene formation, in agreement with the experimental observations. For the side-chain methylation proposal for alkene formation from methylbenzene hydrocarbon-pool species, the theoretical reports are less conclusive, and the barriers reported for the rate limiting steps are close to 200 kJ mol^{-1}.[120, 121] These values are rather high, and they might suggest that side chain methylation is of less importance. Interestingly, methylation, either on an exocyclic double bond or directly on the aromatic ring, is suggested to be the rate-determining step in several reports.[118, 121–123] However, experimental work on the co-reaction of methanol and benzene has shown that the very highest methylated benzenes are readily formed as the dominant species by simple methylations at reaction temperatures where alkene formation is insignificant, showing that methylation is quicker than the decomposition (via the paring route) or further reaction (via side-chain methylation) of these species according to the hydrocarbon-pool mechanism.[83, 125, 126]

4. Deactivation by Carbon Deposition

Discussions of catalyst deactivation by carbon deposition is often restricted to graphitic species, termed “coke”, which block active sites or channels in the catalyst. However, any molecule which is too large, or has too high proton affinity, to diffuse through the microporous channels may block the access to and from active sites in zeolitic catalysts, thereby leading to deactivation. In the following, we will use the term “hydrocarbon residues” to describe this type of deactivating species.

The importance of hydrocarbon residues versus graphitic carbon for catalyst deactivation depends on catalyst topology (Section 4.2), but also on temperature. Schulz reported that for a H-ZSM-5 catalyst, severe deactivation was caused by alkylated benzene molecules, identified mainly as ethyltrimethylbenzene and isopropyldimethylbenzene, during MTH testing at 270 and 290 °C.[127] Subsequent temperature-programmed desorption (TPD) of the used catalyst revealed dealkylation of those molecules at temperatures above 350 °C, leading to desorption of alkenes and lighter polymethylated benzenes, and leaving the catalyst free of any carbon-containing residues. This observation led Schulz to suggest that the alkylation–dealkylation equilibrium of benzene is shifted towards the alkene-forming side at temperatures above 350 °C, and that deactivation of this topology is caused by external coke at higher temperatures.[127] Increased temperature further led to longer catalyst lifetimes and less retained hydrocarbons in/on the catalyst; temperature-programmed oxidation (TPO) of used catalyst led to 10 % weight loss after testing at 290 °C, and only 0.3 % weight loss after testing at 380 °C. The corresponding lifetimes were approximately 0.5 h and 400 h, respectively. Further temperature increase to 480 °C gave a slight decrease in catalyst lifetime.

For H-SAPO-34 and its topological analogue H-SSZ-13, a similar effect of temperature on the nature and amount of hydrocarbon residues is observed. Bleken et al. reported that for tests performed at 300–400 °C, the amount of hydrocarbon residues observed by TPO after 25 min testing decreased from 16 % to 6 % for H-SAPO-34, and from 20 % to 9 % for H-SSZ-13 with increasing test temperature.[23] For H-SAPO-34, the retained hydrocarbons observed after 25 min on stream shifted from 70 % bicyclic and 30 % monocyclic arenes at 300 °C, to 30 % bicyclic and 70 % monocyclic arenes at 400 °C. The methanol conversion capacity of the H-SAPO-34 catalyst increased from 1 to 22 g methanol per gram catalyst in the same temperature range. A similar pattern was observed for H-SSZ-13, although even tricyclic arenes were observed in that case, and the optimum in lifetime and lighter hydrocarbon residues were achieved at 350 °C. These studies serve to illustrate how compounds which are recognized as reaction intermediates in one combination of reaction conditions and catalyst topology (See Section 3.2) may serve as deactivating species for other reaction conditions and catalyst topologies.

4.1. Coke Origin

Conversion versus time on-stream curves for the MTH reaction in fixed-bed reactors generally take an S form, irrespective of catalyst topology, with a period of full conversion followed by rather rapid, then declining, deactivation (see for example Refs [23], [120]–[129]). This shape, called delayed breakthrough, is typical of a situation in which the reactions, and also those leading to deactivating species, occur in a narrow zone of the bed.[130] Several studies of H-SAPO-34 and H-ZSM-5 catalysts have shown a coking pattern in accordance with an autocatalytic behavior of the MTH reaction; that is, no coke deposits in the very first part of the bed (MeOH–DME equilibration), followed by a deactivated, coked zone, and finally an active zone.[127], [131], [132]

Together, this set of studies indicates that carbon deposition is mainly linked with reactions involving methanol, and that interconversion reactions among the products (alkenes, alkanes, and arenes) contribute less to catalyst deactivation. In line with these observations, Keil underlined the importance of operating the MTH reactor with contact times well in excess of the critical contact time for obtaining full conversion to prolong the on-stream periods between each regeneration cycle.[128] Among models for the deactivation curve, some are simple, based on methanol conversion alone, with a positive correlation between conversion level and deactivation rate,[129, 133] while others take into account the contribution of product groups (see Ref. [128] and references therein). In either case, good agreement is observed with experimental data, in favor of the simpler models.

4.2. Topology Influence

There is current consensus that monocyclic arenes are reaction intermediates that contribute to increased reaction rates in wide-pore and cavity type topologies as well as in 3D, medium pore zeolites, especially at moderate temperatures (Section 3.2). With the formation of bicyclic arenes, however, the product formation rate of methanol–arene reactions decrease significantly (Section 3.2). Therefore, any arene containing two or more rings may be considered a deactivating species in the MTH reaction.

The mechanism of polycyclic arene formation is not yet fully understood. Sassi et al. observed the formation of tetrahydrodimethylnaphthalene during co-reaction of methanol and various methylbenzenes over H-beta zeolite and suggested that the second aromatic ring is formed by coupling of two isopropyl substituents on the first benzene ring.[76] Bjørgen et al. fed hexamethylbenzene over H-beta zeolite and reported that dihydrotrimethylnaphthalene, which has the same number of carbon atoms as the heptamethylbenzenium ion, was the first bicyclic compound formed.[82] Furthermore, isotopic labeling experiments led to similar isotopomer distribution for those two compounds. The authors suggested that the heptaMB$^+$ ion may be an important intermediate not only for gaseous product formation but also for coke formation in this zeolite. Recently, Bjørgen et al. performed co-feeding studies of ^{13}C-methanol and ^{12}C-benzene over three 12-ring topologies (H-beta, H-MCM-22, and H-mordenite) and reported that the bicyclic compounds formed during deactivation contained a higher fraction of unlabeled carbon than the heptaMB$^+$ ion, in support of Sassi's hypothesis.[125] However, trimethylnaphtalene was observed to be the lowest bicyclic compound formed in all topologies, and this observation is not easily explained by the benzene alkylation model.[125] The ensemble of experimental evidence might suggest that both mechanisms contribute to the formation of polycyclic arenes. In any case, sufficient space for bicyclic arene formation is required, and from studies of effluent products and hydrocarbon residues there seems to be a cut-off in polycyclic arene formation between three-dimensional 12-ring structures (BEA), one-dimensional 12-ring structures (AFI), and three-dimensional 8-ring window/12-ring cavity structures (CHA) on one hand,[74, 82, 83, 134] and three-dimensional 10-ring structures without trap cavities (MFI) on the other.[102, 135] It is well-documented that H-SAPO-34 deactivates far more rapidly than H-ZSM-5, and several authors have suggested that the reason is formation of polycyclic arenes in the spacious cavities of H-SAPO-34, while only monocyclic arenes are formed in H-ZSM-5.[69, 72, 74, 102] Bjørgen et al. further reported that there was no correlation between hydrocarbon residues, which were too large to diffuse through the channels (penta- and hexamethylbenzene) and deactivation during MTH testing of H-ZSM-5 at 370 °C,[102] and concluded that for this topology, external coke was the only plausible cause of the observed activity loss with time on stream, in agreement with Schulz (Section 4.1).[127]

Direct comparisons between deactivation rates of various topologies are often complicated by simultaneous variations of other parameters that are known to influence catalyst deactivation, such as crystal size, acid strength, and acid site density (Section 4.3). Two (quasi-)single-parameter variation studies, where materials with similar crystal size, acid strength, and acid site density but varying topologies were compared, have recently been published. Bleken et al.[135] compared four 3D 10-ring topologies, two with extended channel intersections (IMF, TUN) and two with smaller intersections (MFI, MEL). All materials had similar channel sizes. The topologies with larger intersections deactivated much more rapidly than those with smaller intersections (Figure 16). Moreover, the topologies with extended channel intersections contained much more, and heavier, hydrocarbon residues, thus clearly demonstrating the correlation between topology and deactivation owing to sterically demanding molecules formed in internal cavities. On the other hand, the effluent product spectrum was strikingly similar for the four samples, as expected for samples with similar dimensionality and pore size (Section 3.2, Figure 15).[135] In another study, Park et al. compared four topologies with 8-ring windows and varying cavity sizes, H-SAPO-34 (CHA), UZM-12 (ERI), UZS-9 (LTA), and UZM-5 (UFI), as MTH catalysts.[136] Also here it was observed that the topologies that deactivated more rapidly contained heavier polycyclic arenes after testing than those that deactivated less rapidly.[136] It should be noted, however, that deactivation is not necessarily initiated by polycylic arene formation. In a transient isotopic study of H-SAPO-34, Hereijgers et al. observed that onset of deactivation started before the formation of such polycycles, and suggested that initial deactivation was caused by (gaseous) product molecules that were too bulky to diffuse out of the catalyst cavities and remained in the cavities, eventually hindering diffusion of smaller reactant and product molecules, which would subsequently undergo sequential reactions leading to polycyclic arenes and alkanes.[112]

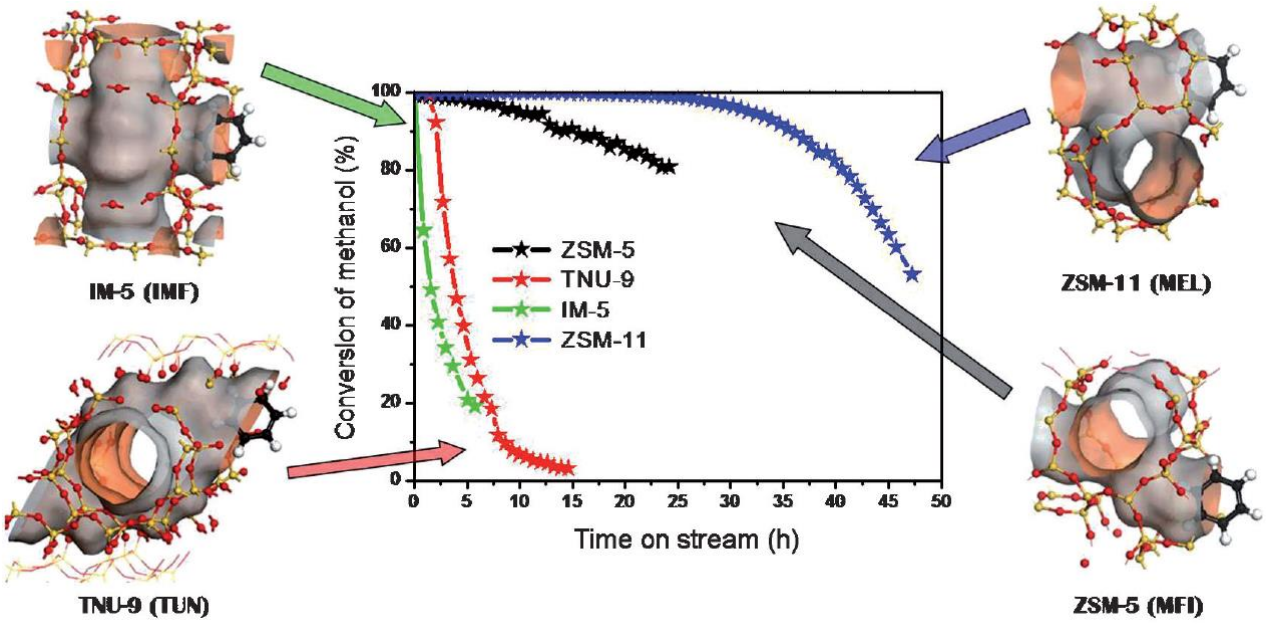

Figure 16. Conversion versus time on stream curves for the MTH reaction over four 3D 10-ring topologies with varying channel intersection size. From Ref. [135].

4.3. Acid Strength and Acid Site Density

Several authors have reported more rapid catalyst deactivation with a higher acid strength and higher acid site density (see for example Ref. [24] and Refs [137–141]). Guisnet and co-workers

elegantly explained these effects in general terms:142 "*The following could be expected on the role of the acidity characteristics: (i) the stronger the acidic sites, the faster the chemical steps and the more pronounced the retention of coke precursors and coke molecules, hence the faster the coking rate; (ii) the higher the density of the acid sites, thus the closer these sites are to each other, the larger the number of successive chemical steps undergone by reactant molecules along the diffusion path within the zeolite crystallites and the more favorable the condensation reactions, hence the faster the coking rate.*" This statement may also serve to explain the more rapid deactivation of larger, versus smaller, zeolite or zeotype crystals, which is well-documented in earlier works143, 144 and substantiated by recent works showing that only the outer part of the zeolitic crystal is active in the MTH reaction.112, 145

Some authors have suggested that coke formation in catalysts with higher acid strength is further enhanced by a higher selectivity towards intermolecular hydride transfer reactions in such catalysts.137 As intramolecular hydride transfer reactions are part of the alkene-forming cycle from polymethylated arene molecules (Section 3.2, Figure 10), the elucidation of whether higher product formation capacities could be obtained by using isostructural zeotypes with lower acid strength is complicated, and require single-parameter variation studies. Bleken et al. recently performed a comparative study of two CHA analogues, H-SSZ-13 and H-SAPO-34, with similar acid site density and crystal size, but with significantly different acid strength (See Section 2).23 The catalysts were tested at 300 to 425 °C, and they behaved very similarly, with near-identical initial product spectra and the same type of hydrocarbons retained in the catalyst pores during reaction. H-SSZ-13 had a higher activity and more rapid deactivation than H-SAPO-34, in line with its higher acid strength. An interesting observation was that the conversion capacity of H-SSZ-13 was higher than for H-SAPO-34 at lower temperatures (see Figure 17), and that the optimum temperature of reaction was shifted to lower temperatures for this catalyst, thus suggesting that the more acidic H-SSZ-13 could be an interesting alternative to H-SAPO-34 as MTO catalyst.23 However, to finally settle the question of intrinsic coke formation selectivity versus acid strength, it would be necessary to compare isotopological samples with larger pore sizes, to reduce the influence of shape selectivity.

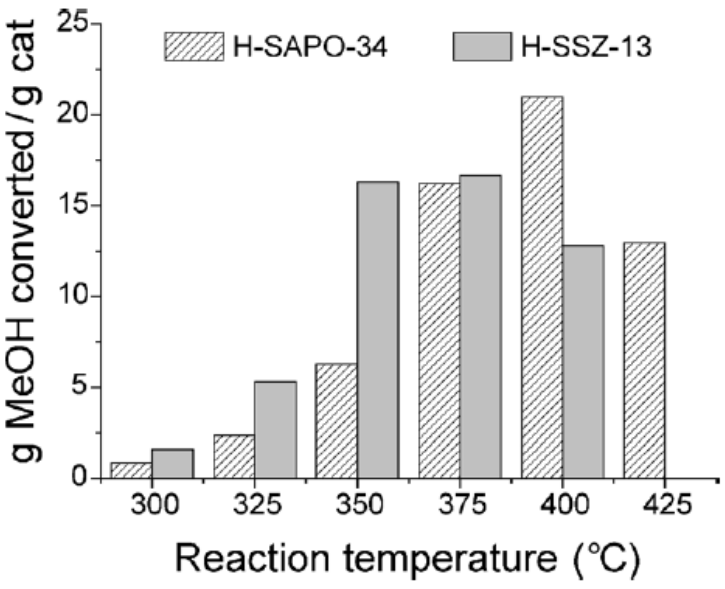

Figure 17. Methanol conversion capacity in H-SAPO-34 and H-SSZ-13. From Ref. 23.

4.4. Effects of Coke Formation on Catalyst Performance

In dense catalysts, which are not affected by diffusion, deactivation is often associated with gradual coverage of active sites, and may be considered simply as a loss of contact time with time on-stream.[146] Janssens[129] recently published time on-stream measurements for a series of H-ZSM-5 catalysts, and suggested that the same assumption could be made for this system. Such a model implies that catalyst selectivity is not affected by deactivation, and for H-ZSM-5, indications exist that this may indeed be the case. Based on a method developed by Abbot and Wojciekowski, product yield versus conversion plots for fresh and partly deactivated H-ZSM-5 catalysts have been reported for 1-hexane cracking,[147] ethene oligomerization,[148] and MTH.[149] All of the studies indicated that deactivation does not affect product selectivity over this topology, in line with Janssens' model.[129]

For the archetypical MTO catalyst, H-SAPO-34, a more complex dependence of product selectivity on deactivation is observed. Several authors have reported an enhanced ethene- to-propene ratio with increasing time on-stream for this topology.[26, 73, 112, 128, 143, 144] Recent studies using $^{12}C/^{13}C$ methanol switching for fresh, partly deactivated, and close to fully deactivated H-SAPO-34 catalysts strongly suggested that the reason is enhanced diffusion restrictions owing to coke formation, that is, product shape selectivity, while hexamethylbenzene remains the main aromatic reaction intermediate during the full induction–conversion–deactivation cycle.[112]

The observed difference in deactivation influence on product selectivity for MFI and CHA topologies reflects the relative importance of external versus internal coke formation, and the ability of product molecules to diffuse past other molecules which are trapped in the zeolite channels and cavities, for each topology. In MFI, external coke is concluded to be the major contributor to catalyst deactivation. Furthermore, in the case of internal coke formation, a penta- or hexamethylbenzene molecule would fill the channel or channel intersection completely and hinder any other molecule from entering that channel. Coke formation therefore completely blocks the access to any active site in the coked channel. In the CHA topology, however, internal coke is of major importance for catalyst deactivation. Furthermore, its large cavities are spacious enough for an alkene molecule to pass by even a bi- or polycyclic aromatic compound/coke precursor, thus giving access to active sites at the interior of a coked cavity.

5. Other Reactants

In their initial paper, Chang and Silvestri reported test data for reactants, such as higher alcohols, ketones, aldehydes, and mercaptans over H-ZSM-5 zeolite.[38] In general, they found that the higher alcohols gave similar product distribution as methanol, while the product distribution from other classes of molecules differed to a smaller or larger extent. The use of other reactants in MTH-like reactions has subsequently focused on two classes of reactants, that is, higher alcohols and methyl halides.

5.1. Higher Alcohols

When ethanol is used as a feed, essentially the same hydrocarbon molecules are found in the product as in MTH, but the species trapped inside the zeolite contain a higher amount of ethyl-substituted molecules.[150, 151] Furthermore, ethene can be directly formed from ethanol on a zeolite catalyst[152, 153] and this reaction has no direct counterpart with a methanol feed. Owing to

the increased interest in production and use of bioethanol, the conversion of ethanol to hydrocarbons has received more attention in the last 2–3 years, as this is a way to produce hydrocarbons, such as ethene, propene, or aromatics, from a bioethanol feedstock.[154–170]

In the conversion of isopropanol, a different situation occurs. In fact, this system resembles an alkene oligomerization system, as in the MOGD process (Section 1.1.2). The selectivity towards alkanes and aromatics becomes significantly lower, compared to a methanol or ethanol feed, while the selectivity for alkenes increases.[171] This suggests that the amount of aromatics inside the zeolite channels is lower. At the same time, the catalyst lifetime becomes more than 25 times longer,[171] which suggests that aromatic compounds play an important role for the deactivation of the zeolite catalysts.

5.2. Methyl Halides

Methyl halides may be formed either from methane by reaction with molecular halogens (see for example Refs [172–176]), or from biomass.[177] When considering natural gas as the source of higher hydrocarbons, methyl halides have the advantage that they may be formed directly from methane without the synthesis gas-forming step required for methanol synthesis, and with relatively high yields compared to other direct conversion processes.[178]

Methyl halide conversion to hydrocarbons has been under study since the mid-1980s. Taylor et al. pioneered the field, focusing on MeCl conversion over H-ZSM-5.[179–181] More recent studies have focused on the CHA topology, that is, either protonated or ion-exchanged H-SAPO-34, for MeCl[182–188] or MeBr[187, 189] conversion. Irrespective of the topology or halogen chosen, the methyl halide conversion to hydrocarbons gives strikingly similar product selectivities to methanol conversion over the same topology.[179–189] Transient isotopic-labeling studies over H-SAPO-34 catalyst recently indicated that the reaction mechanism is also similar, with hexamethylbenzene as a main intermediate in both cases.[178] A main difference between methanol and methyl halides as reactants is the significantly lower conversion observed for the methyl halides. Svelle et al. reported that for a H-SAPO-34 catalyst that was preactivated with a propene pulse, the initial methanol conversion was 25 times higher than either methyl chloride or methyl bromide conversion at 350 °C.[187] Theoretical studies suggest the reason is the lower proton affinity of methyl chloride and methyl bromide compared to methanol (647, 664, and 761 kJ mol^{-1}, respectively[190]),[191, 192] and this was recently supported by co-feeding studies of ^{13}C-labeled methyl chloride with ethene and propene.[178] Svelle et al. further observed a nonlinear increase in methyl halide conversion with increasing contact time. A plausible explanation for this observation is reaction between HCl co-produced with the alkenes and the catalyst lattice. Su et al. used in situ FTIR spectroscopy and observed the formation of P—OH bonds when feeding either HCl or MeCl over H-SAPO-34 catalysts at 350–400 °C. They suggested that HCl may break Al—O—P bonds in the catalyst, leading to the formation of Al—Cl and P—OH.[186, 193] Loss of Brønsted acid sites was observed by the same treatment; however, the broken bonds seem to heal during subsequent regeneration, leading to unaltered initial activity and conversion capacity of the catalyst during several test cycles.[178]

McFarland et al. studied an integrated process for the conversion of methane with bromine to higher hydrocarbons, with MeBr as intermediate product.[194–197] They observed more rapid deactivation in the integrated process than for a separate MeBr to hydrocarbons reaction over H-ZSM-5, and suggested it was due to the presence of overbrominated methane.[194] In conjunction with their study, Nilsen et al. performed an isotopic labeling study in which dichloromethane was co-fed with

methyl chloride over H-SAPO-34 with the aim of elucidating whether coke formation from over-chlorinated products was mechanistically separated from the methyl halide to hydrocarbons reaction, and could thereby be avoided by catalyst tailoring. They observed that dichloromethane was instead an integrated part of the methyl chloride to hydrocarbons reaction cycle, where it led to more rapid formation of polycyclic aromatics and coke.198

6. Recent Developments

6.1. Internal Defects

A topic which has been less studied, but is now receiving increasing attention, is the role of lattice defects in zeolite-catalyzed reactions.20–22, 199–206 From a 2D correlation analysis of in situ IR spectroscopy data, Thibault-Starzyk et al. found a correlation between the formation of coke and the presence of silanol defects in the isomerization of *ortho*-xylene over H-ZSM-5.205 It was found that coke deposits were mainly located on non-acidic silanol groups inside the micropore system. A very recent study by Barbera et al., of a large number of H-ZSM-5 batches, showed that although catalyst activity is linearly correlated with the number of active sites, there is no direct correlation between catalyst deactivation and the number of active sites, nor with crystal size (Figure 18).21 However, a linear correlation between deactivation and the relative number of internal and external silanols was demonstrated. The results showed a clear correlation between the deactivation behavior and the intensities for the isolated silanol bands in the IR spectrum at 3726 and 3745 cm^{-1}, corresponding to the internal silanol groups, and the silanol groups on the external surface of the zeolite, respectively. Sazama et al. confirmed the existence of a correlation between framework defects in H-ZSM-5 and the lifetime in MTH by applying a combination of IR and solid-state NMR spectroscopy.20 Apart from purely microporous MFI, Sazama et al. extended the range of investigated materials to so-called hierarchical systems, which contain both micro- and mesopores (see Section 6.2). They concluded that the concentration of framework defects in the final product is largely influenced by the synthesis procedure for mesopore formation and that the beneficial effect of mesoporosity for the MTH reaction can be occluded by the presence of a high concentration of internal defects. A link between the incorporation of mesopores and the resulting effects on the microstructure of MFI had been noticed earlier by researchers from Haldor Topsøe.201, 203

Despite the clear experimental evidence for the importance of internal or framework defects on the deactivation of MFI, the exact mechanism leading to accelerated activity loss during oxygenate conversion to hydrocarbons remains unclear. Barbera et al. discuss a possible stabilization or retention effect of coke precursors, that is, polymethylated benzene, by internal silanols, leading to modified diffusivities for reaction products.21 Sazama et al. explain the formation of internal silanols as a balancing effect to the presence of partially extra-framework aluminum atoms.20 The presence of Al-related electron-acceptor sites would support oligomerization and hydrogen-transfer reactions leading to coke formation.

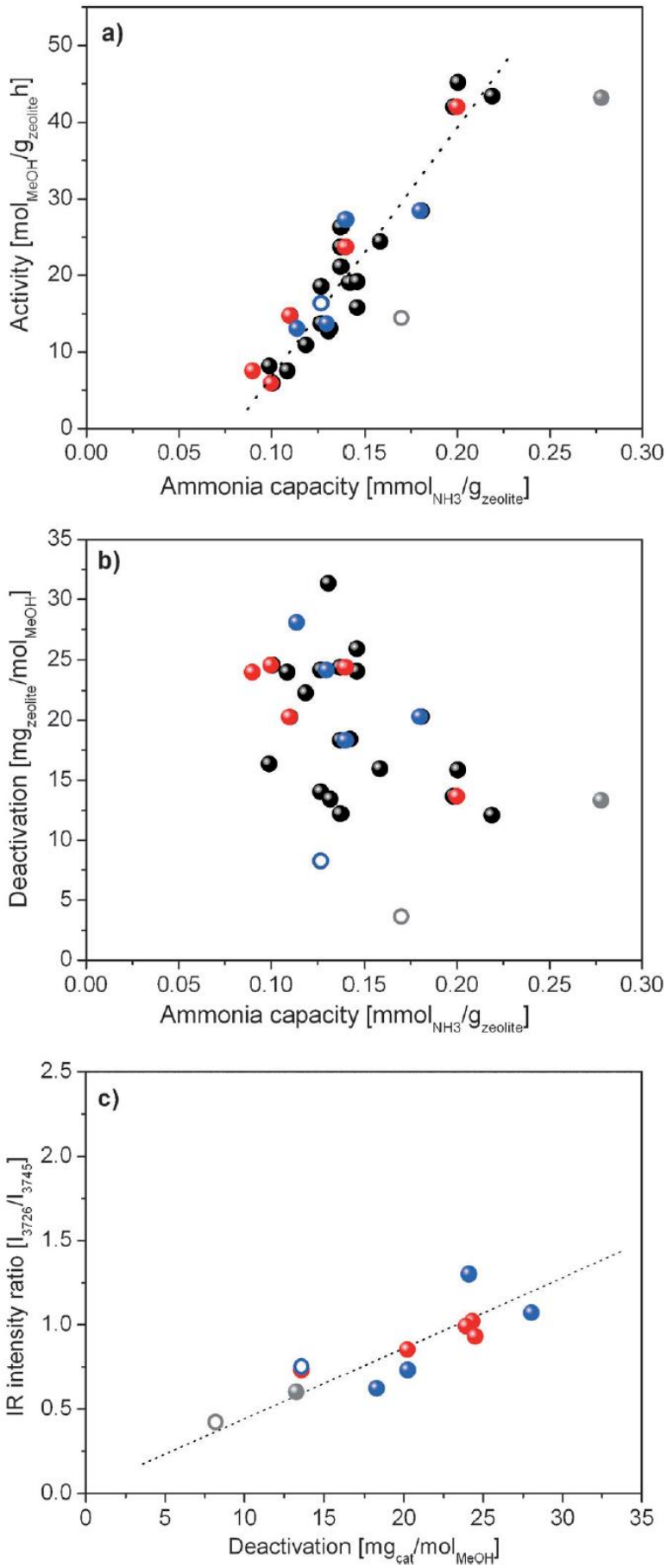

Figure 18. Influence of density of acid sites on a) MTH conversion and b) catalyst deactivation. c) The influence of the relative density of internal defects on catalyst deactivation for MTH reaction over H-ZSM-5 samples. From Ref. 21.

6.2. Mesoporous Zeolites

Ryoo and co-workers recently demonstrated how catalyst deactivation could be restricted by conducting the MTH reaction over H-ZSM-5 nanosheets with unit cell thickness, thereby minimizing the diffusion restrictions of larger catalyst crystals.[207]

A more straightforward strategy to circumvent the inherent diffusion limitations of microporous materials is to introduce a secondary pore system consisting of larger pores, that is, mesopores, resulting in so-called hierarchical zeolites. Various strategies for creating combined micro- and mesoporous materials have been developed. Some studies focus on the introduction of mesopores during synthesis, for example by soft and hard templating routes, while others deal with post synthesis modification by steaming, acid leaching, or alkaline treatment (see Ref. [208] and references therein). While steaming and acid leaching tend to remove Al sites from the framework, alkaline leaching has been shown to remove Si atoms selectively, leaving the catalytically important Al sites unaffected. Alkaline leaching is therefore often termed "desilication". This finding led to a tremendous hype in the last decade, which is reflected in numerous research articles, including extended reviews covering the subject.[209–211] However, only a very limited amount of publications deal with the application of hierarchical zeolites in the MTH reaction. In 2008, Bjørgen et al. reported an increased conversion capacity, that is, the amount of methanol converted per weight of catalyst, by a factor of up to 3.3 for mesoporous MFI samples synthesized by desilication.[212] An increased selectivity towards heavier products (gasoline fraction) was also observed. The results were rationalized by alterations of the acidic properties, mesopore formation, and improved diffusivity. At about the same time Kustova et al. compared differently synthesized mesoporous H-ZSM-5 samples for the MTG reaction, including core–shell particles, and observed similar trends as Bjørgen et al.[209] They pointed out that the different mechanisms of mesopore generation from carbon templating and desilication yield products with a different degree of framework defects, which in turn seem to have an effect on the conversion capacity. A more detailed investigation by Kim et al. in 2010 included a direct method of mesopore generation using organosilane surfactants, together with desilicated and carbon templated mesoporous MFI samples.[213] They highlighted the importance of the Si/Al ratio for the deactivation mode, that is, external versus internal coking and concluded that the conversion capacity of a mesoporous zeolite at a given Si/Al ratio correlates linearly with the external surface area, that is, mesopore surface area. A similar correlation between lifetime and external surface area was obtained by Vennestrøm et al. for mesoporous H-ZSM-5 samples obtained by post-synthesis treatment with guanidium bases.[214]

In a recent contribution, Svelle et al. addressed the complex interplay between the morphological and microstructural properties of H-ZSM-5 crystals and the mechanism of mesopore generation.[22] They concluded that the generalized, simple picture of mesopore formation and catalyst improvement by enhanced diffusion properties requires a detailed knowledge on the microstructure of the hierarchical zeolite sample. Crystal size and morphology, framework defects, and Si/Al ratio need to be considered when the effect of mesopores is to be rationalized in a satisfactory way.

7. Summary and Outlook

The main parameters governing product selectivity in MTH reactions are now largely understood. Product formation takes place over hybrid organic–inorganic sites, the composition of which depends on zeolite topology. In 1D 10-ring structures, alkene intermediates dominate, giving

mainly C_3^+ products and negligible production of aromatics. With increasing pore and/or cavity size, arenes gradually take over as the most important intermediates, leading to higher C_2/C_3 product ratios and an aromatics-rich product mixture, unless the pore/cavity size difference prohibits their diffusion into the gas phase. Increasing pore and cavity sizes further leads to formation of bicyclic arenes. They have lower activity as MTH intermediates than their monocyclic analogues, and are also coke precursors.

With the current commercialization of several MTH processes, the interest in this research field is likely to increase in the coming years, especially in topics of relevance to optimal plant operation and catalyst performance. Although H-ZSM-5 is presently the preferred MTH catalyst, the search for other MTG topologies which give a cut-off at C_9 arenes (Section 2.1), or avoid formation of an aromatic fraction (for example, 1D 10-ring topologies; Section 3.2) will certainly continue. RTH, a 2D 8-ring structure, is one example of novel topologies with interesting MTH product composition.[215]

Zeolites with lower dimensionality are subject to more rapid deactivation.[216] To match the conversion capacity of H-ZSM-5, novel catalyst topologies with 1D or 2D pore structures will call for crystal engineering, for example, nanosized[207] or defect crystals that are susceptible to mesopore formation,[217] to minimize diffusion restrictions.

Long-term catalyst stability is another important issue. Irreversible catalyst deactivation during MTH test–regeneration cycles is documented in several reviews and has been allocated to materials degradation, either by loss of active sites and formation of extra-framework aluminum species (EFAl), or by phase changes, leading to other zeolite topologies, amorphous, and/or dense phases.[24, 26, 218] The topic of irreversible deactivation received significant interest during the 1990s, and an important contribution by Prins and co-workers pointed to the influence of tetrahedral atom strain in (undesired) lattice dealumination.[219] New generations of stability studies will benefit from recent developments of in situ techniques, for example, simultaneous coke and unit-cell dimension measurements by X-ray diffraction, showing lattice strain gradually induced by the coke;[220, 221] confocal fluorescence spectroscopy, showing how the formation rate of hydrocarbon residues is influenced by Si/Al ratio and pore architecture;[141] and NMR spectroscopy studies showing the formation of lattice defects during catalyst pretreatment and testing.[222]

The present understanding of the structure–performance correlation of MTH reactions has potential beyond the optimitation of the title process. One example is the use of kinetic data for individual reaction steps of the MTH cycle (for example, methylation of alkenes and aromatics) as a benchmark for novel quantum-chemical modeling methods.[31] To reach the level of predictability which has been achieved for first principle modeling of metal-based catalysts,[223] it will be necessary to measure the kinetics of individual reactions for a number of different zeolite topologies. Parameter variation studies will be key to the further progress in this field. Even more importantly, while protonated zeolite chemistry is favoring the production of branched hydrocarbons owing to the carbocationic mechanism,[224] the insight in shape selectivity gained from MTH studies adds a new dimension to the design of novel processes involving confined redox-active sites.

Acknowledgements

This publication is part of the inGAP Centre for Research-based Innovation, which receives financial support from the Norwegian Research Council under contract no. 174893.
Dedicated to Professor Stein Kolboe

Biographical Information

The authors (from left to right): Top: M. Bjørgen, P. Beato, T. V. W. Janssens, F. Joensen. Bottom: S. Svelle, K. P. Lillerud, U. Olsbye, S. Bordiga.

References

[1] C. D. Chang, Catal. Rev. Sci. Eng. 1983, 25, 1.
[2] S. Yurchak, Stud. Surf. Sci. Catal. 1988, 36, 251.
[3] C. D. Chang, Catal. Today 1992, 13, 103.
[4] J. Topp-Jorgensen, Stud. Surf. Sci. Catal. 1988, 36, 293.
[5] F. Joensen, P. E. Hojlund Nielsen, M. D. Palis Sorensen, Biomass Conv. Bioref. 2011, 1, 85.
[6] A. A. Avidan, Stud. Surf. Sci. Catal. 1988, 36, 307.
[7] B. V. Vora, T. L. Marker, P. T. Barger, H. R. Nielsen, S. Kvisle, T. Fuglerud, Stud. Surf. Sci. Catal. 1997, 107, 87.
[8] Chem. Eng. News 2005, 83(50), 18.
[9] J. Liang, H. Li, S. Zhao,W. Guo, R.Wang,M. Ying, Appl. Catal. 1990, 64, 31.
[10] H. Koempel, W. Liebner, Stud. Surf. Sci. Catal. 2007, 167, 261.
[11] http://www.iza-structure.org/databases.
[12] A. Zecchina, G. Spoto, S. Bordiga in Handbook of Vibrational Spectroscopy, Vol. 4 (Eds.: J. M. Chalmers, P. R. Griffiths), Wiley, Chichester, UK, 2002, p. 3042.
[13] A. Zecchina, G. Spoto, S. Bordiga, Phys. Chem. Chem. Phys. 2005, 7, 1627.
[14] C. Paz_, S. Bordiga, C. Lamberti, M. Salvalaggio, A. Zecchina, J. Phys. Chem. B 1997, 101, 4740.
[15] S. Bordiga, L. Regli, D. Cocina, C. Lamberti, M. Bjorgen, K. P. Lillerud, J. Phys. Chem. B 2005, 109, 2779.
[16] G. A. V. Martins, G. Berlier, S. Coluccia, H. O. Pastore, G. B. Superti, G. Gatti, L. Marchese, J. Phys. Chem. C 2007, 111, 330.
[17] A. Zecchina, S. Bordiga, J. G. Vitillo, G. Ricchiardi, C. Lamberti, G. Spoto, M. Bjorgen, K. P. Lillerud, J. Am. Chem. Soc. 2005, 127, 6361.
[18] K. Chakarova, K. Hadjiivanov, J. Phys. Chem. C 2011, 115, 4806.
[19] B. Gil, Ł. Mokrzycki, B. Sulikowski, Z. Olejniczak, S. Walas, Catal. Today 2010, 152, 24.
[20] P. Sazama, B. Wichterlova, J. Dedecek, Z. Tvaruzkova, Z. Musilova, L. Palumbo, S. Sklenak,O. Gonsiorova, Microporous Mesoporous Mater. 2011, 143, 87.
[21] K. Barbera, F. Bonino, S. Bordiga, T. V.W. Janssens, P. Beato, J. Catal. 2011, 280, 196.

[22] S. Svelle, L. Sommer, K. Barbera, P. N. R. Vennestrom, U. Olsbye, K. P. Lillerud, S. Bordiga, Y. H. Pan, P. Beato, Catal. Today 2011, 168, 38.
[23] F. Bleken, M. Bjorgen, L. Palumbo, S. Bordiga, S. Svelle, K. P. Lillerud, U. Olsbye, Top. Catal. 2009, 52, 218.
[24] M. Stccker, Microporous Mesoporous Mater. 1999, 29, 3.
[25] C. D. Chang in Shape Selective Catalysis: Chemical Synthesis and Hydrocarbon Processing (Eds.: C. Song, J. M. Garcés, Y. Sugi), ACS, Washington, 2000, p. 96 (ACS Symp. Ser. 738).
[26] P. Barger in Zeolites for Cleaner Technologies, (Eds.: M. Guisnet, J.-P. Wilson), Imperial College Press, London, 2002, p. 239 (Catal. Sci. Ser. Vol. 3).
[27] J. F. Haw, D. M. Marcus in Handbook of Zeolite Science and Technology (Eds: S. M. Auerbach, K. A. Carrado, P. K. Dutta), Marcel Dekker, New York, 2003, p. 833.
[28] D. M. Marcus, M. J. Heyman, Y. M. Blau, D. R. Guenther, J. O. Ehresmann, P. W. Kletnieks, J. F. Haw, Angew. Chem. 2006, 118, 1967; Angew. Chem. Int. Ed. 2006, 45, 1933.
[29] D. M. Marcus, K. A. McLachlan, M. A. Wildman, J. O. Ehresmann, P.W. Kletnieks, J. F. Haw, Angew. Chem. 2006, 118, 3205; Angew. Chem. Int. Ed. 2006, 45, 3133.
[30] P. Magnoux, P. Roger, V. Fouche, N. S. Gnep, M. Guisnet, Stud. Surf. Sci. Catal. 1987, 34, 317.
[31] S. Svelle, C. Tuma, X. Rozanska, T. Kerber, J. Sauer, J. Am. Chem. Soc. 2009, 131, 816.
[32] V. Van Speybroeck, J. Van der Mynsbrugge, M. Vandichel, K. Hemelsoet, D. Lesthaeghe, A. Ghysels, G. B. Marin, M. Waroquier, J. Am. Chem. Soc. 2011, 133, 888.
[33] J. P. van den Berg, J. P. Wolthuizen, J. H. C. van Hooff in Proceedings 5th International Zeolite Conference (Naples) (Ed.: L. V. Rees), Heyden, London, 1980, p. 649.
[34] G. A. Olah, Pure Appl. Chem. 1981, 53, 201.
[35] G. J. Hutchings, F. Gottschalk, M. V. Mich_le, R. Hunter, J. Chem. Soc. Faraday Trans. 1987, 83, 571.
[36] Y. Ono, T. Mori, J. Chem. Soc. Faraday Trans. 1981, 77, 2209.
[37] D. Kagi, J. Catal. 1981, 69, 242.
[38] C. D. Chang, A. J. Silvestri, J. Catal. 1977, 47, 249.
[39] C. D. Chang, J. Catal. 1981, 69, 244.
[40] E. A. Swabb, B. C. Gates, Ind. Eng. Chem. Fund. 1972, 11, 540.
[41] W. Zatorski, S. Kryzanowski, Acta Phys. Chem. 1978, 29, 347.
[42] J. K. A. Clarke, R. Darcy, B. F. Hegarty, E. O_Donoghue, V. Amir-Ebrahimi, J. J. Rooney, J. Chem. Soc. Chem. Commun. 1986, 425.
[43] S. Kolboe, Stud. Surf. Sci. Catal. 1991, 61, 413.
[44] J. Sauer, M. Sierka, F. Haase in Transition State Modeling for Catalysis (Eds.: D. G. Truhlar, K. Morokuma), ACS, Washington, 1999, p. 358 (ACS Symp. Ser. 721).
[45] S. R. Blaszkowski, R. A. van Santen, J. Phys. Chem. 1995, 99, 11728.
[46] S. R. Blaszkowski, R. A. van Santen, J. Am. Chem. Soc. 1997,
119, 5020.
[47] D. Lesthaeghe, V. Van Speybroeck, G. B. Marin, M.Waroquier,
Angew. Chem. 2006, 118, 1746; Angew. Chem. Int. Ed. 2006, 45, 1714.
[48] D. Lesthaeghe, V. Van Speybroeck, G. B. Marin, M.Waroquier, Ind. Eng. Chem. Res. 2007, 46, 8832.
[49] W. Song, D. M. Marcus, H. Fu, J. O. Ehresmann, J. F. Haw, J. Am. Chem. Soc. 2002, 124, 3844.
[50] S. Kolboe, Stud. Surf. Sci. Catal. 1993, 75, 449.
[51] W. Wang, A. Buchholz, M. Seiler, M. Hunger, J. Am. Chem. Soc. 2003, 125, 15260.
[52] C. S. Lo, R. Radhakrishnan, B. L. Trout, Catal. Today 2005, 105, 93.
[53] Y. Jiang, W. Wang, V. R. R. Marthala, J. Huang, B. Sulikowski, M. Hunger, J. Catal. 2006, 238, 21.
[54] W. Wang, M. Hunger, Acc. Chem. Res. 2008, 41, 895.
[55] W. Wang, Y. Jiang, M. Hunger, Catal. Today 2006, 113, 102.
[56] N. Y. Chen, W. J. Reagan, J. Catal. 1979, 59, 123.
[57] S. Kolboe, Stud. Surf. Sci. Catal. 1988, 36, 189.
[58] S. Kolboe, Acta Chem. Scand. Ser. A 1986, 40, 711.
[59] R. M. Dessau, J. Catal. 1986, 99, 111.
[60] R. M. Dessau, R. B. LaPierre, J. Catal. 1982, 78, 136.
[61] T. Mole, J. Whiteside, D. Seddon, J. Catal. 1983, 82, 261.
[62] T. Mole, G. Bett, D, Seddon, J. Catal. 1983, 84, 435.
[63] I. M. Dahl, S. Kolboe, Catal. Lett. 1993, 20, 329.
[64] I. M. Dahl, S. Kolboe, J. Catal. 1994, 149, 458.
[65] I. M. Dahl, S. Kolboe, J. Catal. 1996, 161, 304.
[66] S. Kolboe, I. M. Dahl, Stud. Surf. Sci. Catal. 1995, 94, 427.
[67] P. O. Ronning, O. Mikkelsen, S. Kolboe in Proceedings of the 12th International Zeolite Conference, Vol. 2 (Eds: M. M. J. Treacy, B. K. Marcus, M. E. Bisher, J. B. Higgins), Materials Research Society, Warrendale, 1999, p. 1057.

[68] O. Mikkelsen, P. O. Ronning, S. Kolboe, Microporous Mesoporous Mater. 2000, 40, 95.
[69] B. Arstad, S. Kolboe, Catal. Lett. 2001, 71, 209.
[70] B. Arstad, S. Kolboe, J. Am. Chem. Soc. 2001, 123, 8137.
[71] W. Song, J. F. Haw, J. B. Nicholas, C. S. Henghan, J. Am. Chem. Soc. 2000, 122, 10726.
[72] W. Song, H. Fu, J. F. Haw, J. Phys. Chem. B 2001, 105, 12839.
[73] W. Song, H. Fu, J. F. Haw, J. Am. Chem. Soc. 2001, 123, 4749.
[74] H. Fu, W. Song, J. F. Haw, Catal. Lett. 2001, 76, 89.
[75] J. F. Haw, D. M. Marcus, Catal. Lett. 2005, 34, 41.
[76] A. Sassi, M. A. Wildman, H. J. Ahn, P. Prasad, J. B. Nicholas, J. F. Haw, J. Phys. Chem. B 2002, 106, 2294.
[77] A. Sassi, M. A.Wildman, J. F. Haw, J. Phys. Chem. B 2002, 106, 8768.
[78] J. F. Haw, Phys. Chem. Chem. Phys. 2002, 4, 5431.
[79] J. F. Haw, W. Song, D. M. Marcus, J. B. Nicholas, Acc. Chem. Res. 2003, 36, 317.
[80] P.W. Goguen, T. Xu, D. H. Barich, T.W. Skloss, W. Song, Z. Wang, J. B. Nicholas, J. F. Haw, J. Am. Chem. Soc. 1998, 120, 2650.
[81] J. F. Haw, J. B. Nicholas,W. Song, F. Deng, Z.Wang, T. Xu, C. S. Henghan, J. Am. Chem. Soc. 2000, 122, 4763.
[82] M. Bjorgen, U. Olsbye, S. Kolboe, J. Catal. 2003, 215, 30.
[83] M. Bjorgen, U. Olsbye, D. Petersen, S. Kolboe, J. Catal. 2004, 221, 1.
[84] M. Bjorgen,U. Olsbye, S. Svelle, S. Kolboe, Catal. Lett. 2004, 93, 37.
[85] M. Bjorgen, F. Bonino, S. Kolboe, K.-P. Lillerud, A. Zecchina, S. Bordiga, J. Am. Chem. Soc. 2003, 125, 15 863.
[86] R. F. Sullivan, C. J. Egan, G. E. Langlois, R. P. Sieg, J. Am. Chem. Soc. 1961, 83, 1156.
[87] S. Svelle,M. Bjorgen, S. Kolboe, D. Kuck, M. Letzel, U. Olsbye, O. Sekiguchi, E. Uggerud, Catal. Lett. 2006, 109, 25.
[88] O. Sekiguchi, V. Meyer, M. C. Letzel, D. Kuck, E. Uggerud, Eur. J. Mass Spectrom. 2009, 15, 167.
[89] M. Seiler,W.Wang, A. Buchholz, M. Hunger, Catal. Lett. 2003, 88, 187.
[90] M. Hunger, T. Horvath, J. Am. Chem. Soc. 1996, 118, 12302.
[91] M. Seiler, U. Schenk, M. Hunger, Catal. Lett. 1999, 62, 139.
[92] M. Seiler, W. Wang, M. Hunger, J. Phys. Chem. B 2001, 105, 8143.
[93] W. Wang, M. Seiler, M. Hunger, J. Phys. Chem. B 2001, 105, 12553.
[94] M. Hunger, M. Seiler, A. Buchholz, Catal. Lett. 2001, 74, 61.
[95] T. Xu, D. H. Barich, P. W. Gougen, W. Song, Z. Wang, J. B. Nicholas, J. F. Haw, J. Am. Chem. Soc. 1998, 120, 4025.
[96] R. L. Espinoza, Appl. Catal. 1986, 26, 203.
[97] Ref. [51].
[98] N. Govind, J. Andzelm, K. Reindel, G. Fitzgerald, Int. J. Mol. Sci. 2002, 3, 423.
[99] C. Lo, C. A. Giurumescu, R. Radhakrishnan, B. L. Trout, Mol. Phys. 2004, 102, 281.
[100] H. Schulz, Z. Siwei, H. Kusterer, Stud. Surf. Sci. Catal. 1991, 60, 281.
[101] S. Svelle, F. Joensen, J. Nerlov, U. Olsbye, K. P. Lillerud, S. Kolboe, M. Bjorgen, J. Am. Chem. Soc. 2006, 128, 14770.
[102] M. Bjorgen, S. Svelle, F. Joensen, J. Nerlov, S. Kolboe, F. Bonino, L. Palumbo, S. Bordiga, U. Olsbye, J. Catal. 2007, 248,
195.
[103] Y. V. Kissin, Catal. Rev. 2001, 43, 85.
[104] M. Bjorgen, F. Joensen, K. P. Lillerud, U. Olsbye, S. Svelle, Catal. Today 2009, 142, 90.
[105] M. Bjorgen, K. P. Lillerud, U. Olsbye, S. Svelle, Stud. Surf. Sci. Catal. 2007, 167, 463.
[106] S. Teketel, S. Svelle, K. P. Lillerud, U. Olsbye, ChemCatChem 2009, 1, 78.
[107] S. Teketel, U. Olsbye, K. P. Lillerud, P. Beato, S. Svelle, Microporous Mesoporous Mater. 2010, 136, 33.
[108] Z.-M. Cui, Q. Liu, S.-W. Bain, Z. Ma, W.-G. Song, J. Phys. Chem. C 2008, 112, 2685.
[109] Z.-M. Cui, Q. Liu, Z. Ma, S.-W. Bain,W.-G. Song, J. Catal. 2008, 258, 83.
[110] J. Li, Y. Wei, Y. Qi, P. Tian, B. Li, Y. He, F. Chang, X. Sun, Z. Liu, Catal. Today 2011, 164, 288.
[111] J. Li, Y. Wei, G. Liu, Y. Qi, P. Tian, B. Li, Y. He, Z. Liu, Catal. Today 2011, 171, 221.
[112] B. P. C. Hereijgers, F. Bleken, M. H. Nilsen, S. Svelle, K. P. Lillerud, M. Bjorgen, B. M. Weckhuysen, U. Olsbye, J. Catal. 2009, 264, 77.
[113] S. Svelle, U. Olsbye, F. Joensen, M. Bjorgen, J. Phys. Chem. C 2007, 111, 17981.
[114] B. Arstad, S. Kolboe, O. Swang, J. Phys. Org. Chem. 2004, 17, 1023.
[115] B. Arstad, S. Kolboe, O. Swang, J. Phys. Chem. A 2005, 109, 8914.
[116] B. Arstad, S. Kolboe, O. Swang, J. Phys. Org. Chem. 2006, 19, 81.
[117] B. Arstad, J. B. Nicholas, J. F. Haw, J. Am. Chem. Soc. 2004, 126, 2991.
[118] D. M. McCann, D. Lesthaeghe, P. W. Kletnieks, D. R. Guenther, M. J. Hayman, V. Van Speybroeck, M. Waroquier, J. F. Haw, Angew. Chem. 2008, 120, 5257; Angew. Chem. Int. Ed. 2008, 47, 5179.

[119] D. Lesthaeghe, V. Van Speybroeck, M.Waroquier, Phys. Chem. Chem. Phys. 2009, 11, 5222.
[120] D. Lesthaeghe, A. Horre, M. Waroquier, G. B. Marin, V. Van Speybroeck, Chem. Eur. J. 2009, 15, 10803.
[121] C.-M.Wang, Y.-D.Wang, Z.-K. Xie, Z.-P. Liu, J. Phys. Chem. C 2009, 113, 4584.
[122] C.-M. Wang, Y.-D. Wang, H.-X. Liu, Z.-K. Xie, Z.-P. Liu, J. Catal. 2010, 271, 386.
[123] B. Chan, L. Radom, Can. J. Chem. 2010, 88, 866.
[124] D. Lesthaeghe, J. Van der Mynsbrugge, M. Vandichel, M. Waroquier, V. Van Speybroeck, ChemCatChem 2011, 3, 208.
[125] M. Bjorgen, S. Akyalcin, U. Olsbye, S. Benard, S. Kolboe, S. Svelle, J. Catal. 2010, 275, 170.
[126] W. Song, J. B. Nicholas, A. Sassi, J. F. Haw, Catal. Lett. 2002, 81, 49.
[127] H. Schulz, Catal. Today 2010, 154, 183.
[128] F. J. Keil, Microporous Mesoporous Mater. 1999, 29, 49.
[129] T. V.W. Janssens, J. Catal. 2009, 264, 130.
[130] G. F. Froment, Catal. Rev. Sci. Eng. 2008, 50, 1.
[131] J. F. Haw, D. M. Marcus, Top. Catal. 2005, 34, 41.
[132] M. Kaarsholm, F. Joensen, J. Nerlov, R. Cenni, J. Chaouki, G. S. Patience, Chem. Eng. Sci. 2007, 62, 5527.
[133] P. H. Schipper, F. J. Krambeck, Chem. Eng. Sci. 1986, 41, 1013.
[134] D. M. Marcus,W. Song, L. L. Ng, J. F. Haw, Langmuir 2002, 18, 8386.
[135] F. Bleken, W. Skistad, K. Barbera, M. Kustova, S. Bordiga, P. Beato, K. P. Lillerud, S. Svelle, U. Olsbye, Phys. Chem. Chem. Phys. 2011, 13, 2539.
[136] J. W. Park, J. Y. Lee, K. S. Kim, S. B. Hong, G. Seo, Appl. Catal. A 2008, 339, 36.
[137] L.-T. Yuen, S. I. Zones, T. V. Harris, E. J. Gallegos, A. Auroux, Microporous Mater. 1994, 2, 105.
[138] S. Wilson, P. Barger, Microporous Mesoporous Mater. 1999, 29, 117.
[139] Q. Zhu, J. N. Kondo, R. Ohnuma, Y. Kubota, M. Yamaguchi, T. Tatsumi, Microporous Mesoporous Mater. 2008, 112, 153.
[140] I. M. Dahl, H. Mostad, D. Akporiaye, R. Wendelbo, Microporous Mesoporous Mater. 1999, 29, 185.
[141] D. Mores, J. Kornatowski,U. Olsbye, B. M.Weckhuysen, Chem. Eur. J. 2011, 17, 2874.
[142] M. Guisnet, L. Costa, F. R. Ribeiro, J. Mol. Catal. A 2009, 305, 69.
[143] D. Chen, K. Moljord, T. Fuglerud, A. Holmen, Microporous Mesoporous Mater. 1999, 29, 191.
[144] I. M. Dahl, R. Wendelbo, A. Andersen, D. Akporiaye, H. Mostad, T. Fuglerud, Microporous Mesoporous Mater. 1999, 29, 159.
[145] D. Mores, E. Stavitski, M. H. F. Kox, J. Kornatowski, U. Olsbye, B. M. Weckhuysen, Chem. Eur. J. 2008, 14, 11320.
[146] C. H. Bartholomew, Chem. Eng. 1984, 91, 96.
[147] J. Abbot, B. W. Wojciechowski, Can. J. Chem. Eng. 1985, 63, 451.
[148] D. Chen, H. P. Rebo, K. Moljord, A. Holmen, Ind. Eng. Chem. Res. 1997, 36, 3473.
[149] F. Bleken, PhD Thesis, University of Oslo, 2011.
[150] R. Johansson, S. L. Hruby, J. Rass-Hansen, C. H. Christensen, Catal. Lett. 2009, 127, 1.
[151] F. F. Madeira, N. S. Gnep, P. Magnoux, S. Maury, N. Cadran, Appl. Catal. A 2009, 367, 39.
[152] M. Katoh, T. Yamazaki, N. Kikuchi, Y. Okada, T. Yoshikawa, M. Wada, Kagaku Kogaku Ronbunshu 2008, 34, 396.
[153] Q. Zhu, J. N. Kondo, S. Inagaki, T. Tatsumi, Top. Catal. 2009, 52, 1272.
[154] W. Xia, A. Takahashi, I. Nakamura, H. Shimada, T. Fujitani, J. Mol. Catal. A 2010, 328, 114.
[155] F. Wang, M. Luo, W. Xiao, X. Cheng, Y. Long, Appl. Catal. A 2011, 393, 161.
[156] T. Tsuchida, T. Yoshioka, S. Sakuma, T. Takeguchi, W. Ueda, Ind. Eng. Chem. Res. 2008, 47, 1443.
[157] V. F. Tret_yakov, A. S. Lermontov, Y. I. Makarfi, M. S. Yakimova, N. A. Frantsuzova, L. M. Koval', V. I. Erofeev, Chem. Technol. Fuels Oils 2008, 44, 409.
[158] Z. Song, A. Takahashi, I. Nakamura, T. Fujitani, Appl. Catal. A 2010, 384, 201.
[159] Z. Song, A. Takahashi, N. Mimura, T. Fujitani, Catal. Lett. 2009, 131, 364.
[160] Y. I. Makarfi, M. S. Yakimova, A. S. Lermontov, V. I. Erofeev, L. M. Koval, V. F. Tretiyakov, Chem. Eng. J. 2009, 154, 396.
[161] S. Ivanova, E. Vanhaecke, L. Dreibine, B. Louis, C. Pham, C. Pham-Huu, Appl. Catal. A 2009, 359, 151.
[162] T. Inoue,M. Itakura, H. Jon,Y. Oumi, A. Takahashi, T. Fujitani, T. Sano, Microporous Mesoporous Mater. 2009, 122, 149.
[163] M. Inaba, K. Murata, I. Takahara, K. Inoue, J. Chem. Technol. Biotechnol. 2011, 86, 95.
[164] M. Inaba, K. Murata, I. Takahara, React. Kinet. Catal. Lett. 2009, 97, 19.
[165] M. Inaba, K. Murata, M. Saito, I. Takahara, Green Chem. 2007, 9, 638.
[166] M. Inaba, K. Murata, M. Saito, I. Takahara, React. Kinet. Catal.
Lett. 2006, 88, 135.

[167] D. Goto, Y. Harada, Y. Furumoto, A. Takahashi, T. Fujitani, Y. Oumi, M. Sadakane, T. Sano, Appl. Catal. A 2010, 383, 89.
[168] R. V. Ermakov, V. A. Plakhotnik, Petrol. Chem. 2008, 48, 1.
[169] X. Cheng, Y. Jin, J.Wang, J. Guo, Y. Long,W. Xiao, Petrochem. Technol. 2008, 37, 548.
[170] J. Bi, X. Guo, M. Liu, X. Wang, Catal. Today 2010, 149, 143.
[171] U. V. Mentzel, S. Shunmugavel, S. L. Hruby, C. H. Christensen, M. S. Holm, J. Am. Chem. Soc. 2009, 131, 17009.
[172] S. G. Podkolzin, E. E. Stangland, M. E. Jones, E. Peringer, J. A. Lercher, J. Am. Chem. Soc. 2007, 129, 2569.
[173] E. Peringer, M. Salzinger, M. Hutt, A. A. Lemonidou, J. A. Lercher, Top. Catal. 2009, 52, 1220.
[174] G. A. Olah, B. Gupta, M. Farina, J. D. Felberg, W. M. Ip, A. Husain, R. Karpeles, K. Lammertsma, A. K. Melhotra, N. J. Trivedi, J. Am. Chem. Soc. 1985, 107, 7097.
[175] V. Degirmenci, A. Yilmaz, D. Uner, Catal. Today 2009, 142, 30.
[176] I. M. Lorkovic, S. Sun, S. Gadewar, A. Breed, G. S. Macala, A. Sardar, S. E. Cross, J. H. Sherman, G. D. Stucky, P. C. Ford, J. Phys. Chem. A 2006, 110, 8695.
[177] T. S. Bayer, D. M. Widmayer, K. Temme, E. A. Mirsky, D. V. Santi, C. A. Voigt, J. Am. Chem. Soc. 2009, 131, 6508.
[178] U. Olsbye, O. V. Saure, N. B. Muddada, S. Bordiga, C. Lamberti, M. H. Nilsen, S. Svelle, Catal. Today 2011, 171, 211.
[179] C. E. Taylor, R. P. Noceti, R. R. Schehl, Stud. Surf. Sci. Catal. 1988, 36, 483.
[180] C. E. Taylor, R. P. Noceti, Proc. Int. Congr. Catal. 1988, 2, 990.
[181] C. E. Taylor, Stud. Surf. Sci. Catal. 2000, 130D, 3633.
[182] D. Jaumain, B.-L. Su, Catal. Today 2002, 73, 187.
[183] D. Jaumain, B.-L. Su, J. Mol. Catal. A 2003, 197, 263.
[184] B.-L. Su, D. Jaumain in Proceedings of the 12th International Zeolite Conference (Eds.: M. M. J. Treacy, B. K. Marcus, M. E. Bisher, J. B. Higgins), Materials Resarch Society, Warrendale, 1998, p. 2689.
[185] B.-L. Su, D. Jaumain in Proceedings of the 12th International Zeolite Conference (Eds.: M. M. J. Treacy, B. K. Marcus, M. E. Bisher, J. B. Higgins), Materials Resarch Society, Warrendale, 1998, p. 2681.
[186] Y.Wei, D. Zhang, L. Xu, Z. Liu, B.-L. Su, J. Catal. 2006, 238, 46.
[187] S. Svelle, S. Aravinthan, M. Bjorgen, K. P. Lillerud, S. Kolboe, I. M. Dahl, U. Olsbye, J. Catal. 2006, 241, 243.
[188] M. H. Nilsen, S. Svelle, S. Aravinthan,U. Olsbye, Appl. Catal. A 2009, 367, 23.
[189] A. Zhang, S. Sun, Z. J. A. Komon, N. Osterwalder, S. Gadewar, P. Stoimenov, D. J. Auerbach, G. D. Stucky, E. W. McFarland, Phys. Chem. Chem. Phys. 2011, 13, 2550.
[190] S. G. Lias, J. F. Liebman, R. D. J. Levin, J. Phys. Chem. Ref. Data 1984, 13, 695.
[191] S. Svelle, S. Kolboe, U. Olsbye, O. Swang, J. Phys. Chem. B 2003, 107, 5251.
[192] F. Bleken, S. Svelle, K. P. Lillerud, U. Olsbye, B. Arstad, O. Swang, J. Phys. Chem. A 2010, 114, 7391.
[193] Y.Wei, D. Zhang, Z. Liu, B.-L. Su, Chem. Phys. Lett. 2007, 444, 197.
[194] I. Lorkovic, M. Noy,M.Weiss, J. Sherman, E. McFarland, G. D. Stucky, P. C. Ford, Chem. Commun. 2004, 566.
[195] I. M. Lorkovic, A. Yilmaz, G. A. Yilmaz, X.-P. Zhou, L. E. Laverman, S. Sun, D. J. Schaefer, M. Weiss, M. L. Noy, C. I. Cutler, J. H. Sherman, E. W. McFarland, G. D. Stucky, P. C. Ford, Catal. Today 2004, 98, 317.
[196] I. M. Lorkovic, M. L. Noy, W. A. Schenck, C. Belon, M. Weiss, S. Sun, J. H. Sherman, E.W. McFarland, G. D. Stucky, P. C. Ford, Catal. Today 2004, 98, 589.
[197] A. Breed, M. F. Doherty, S. Gadewar, P. Grosso, I. M. Lorkovic, E. W. McFarland, M. J. Weiss, Catal. Today 2005, 106, 301.
[198] Ref. [188].
[199] S. Bordiga, I. Roggero, P. Ugliengo, A. Zecchina, V. Bolis, G. Artioli, R. Buzzoni, G. Marra, F. Rivetti, G. Spanò, C. Lamberti, J. Chem. Soc. Dalton Trans. 2000, 3921.
[200] B. Gil, K. Mierzynska, M. Szczerbinska, J. Datka, Microporous Mesoporous Mater. 2007, 99, 328.
[201] M. S. Holm, S. Svelle, F. Joensen, P. Beato, C. H. Christensen, S. Bordiga, M. Bjorgen, Appl. Catal. A 2009, 356, 23.
[202] G. J. Hutchings, G.W. Watson, D. J. Willock, Microporous Mesoporous Mater. 1999, 29, 67.
[203] M. Kustova, M. S. Holm, C. H. Christensen, Y. H. Pan, P. Beato, T. V.W. Janssens, F. Joensen, J. Nerlov, Stud. Surf. Sci. Catal. 2008, 174, 117.
[204] S. Shih, J. Catal. 1983, 79, 390.
[205] F. Thibault-Starzyk, A. Vimont, J. P. Gilson, Catal. Today 2001, 70, 227.
[206] A. Zecchina, S. Bordiga, G. Spoto, L. Marchese, G. Petrini, G. Leofanti, M. Radovan, J. Phys. Chem. 1992, 96, 4991.
[207] M. Choi, K. Na, J. Kim, Y. Sakamoto, O. Terasaki, R. Ryoo, Nature 2009, 461, 828.
[208] L. Sommer, D. Mores, S. Svelle,M. Stccker, B. M.Weckhuysen, U. Olsbye, Microporous Mesoporous Mater. 2010, 132, 384.

[209] M. Kustova, K. Egeblad, C. H. Christensen, A. L. Kustov, C. H. Christensen, Stud. Surf. Sci. Catal. 2007, 170, 267.
[210] J. P_rez-Ram_rez, C. H. Christensen, K. Egeblad, C. H. Christensen, J. C. Groen, Chem. Soc. Rev. 2008, 37, 2530.
[211] M. S. Holm, E. Taarning, K. Egeblad, C. H. Christensen, Catal. Today 2011, 168, 3.
[212] M. Bjorgen, F. Joensen, M. Spangsberg Holm, U. Olsbye, K. P. Lillerud, S. Svelle, Appl. Catal. A 2008, 345, 43.
[213] J. Kim, M. Choi, R. Ryoo, J. Catal. 2010, 269, 219.
[214] P. N. R. Vennestrøm, M. Grill, M. Kustova, K. Egeblad, L. F. Lundegaard, F. Joensen, C. H. Christensen, P. Beato, Catal. Today 2011, 168, 71.
[215] T. Yokoi, M. Yoshioka, H. Imai, T. Tatsumi, Angew. Chem. 2009, 121, 10068; Angew. Chem. Int. Ed. 2009, 48, 9884.
[216] D. Chen, K. Moljord, A. Holmen in Deactivation and Regeneration of Zeolite Catalysts (Eds.: M. Guisnet, F. R. Ribeiro), Imperial College Press, London, 2011, p. 269 (Catalytic Science Series Vol 9).
[217] L. Sommer, S. Svelle, K. P. Lillerud, M. Stçcker, B. M. Weckhuysen, U. Olsbye, Langmuir 2010, 26, 16510.
[218] M. Guisnet in Deactivation and Regeneration of Zeolite Catalysts (Eds.: M. Guisnet, F. R. Ribeiro), Imperial College Press, London, 2011, p. 217 (Catalytic Science Series Vol 9).
[219] M. Müller, G. Harvey, R. Prins, Microporous MesoporousMater. 2000, 34, 135.
[220] D. S. Wragg, R. E. Johnsen, M. Balasundaram, P. Norby, H. Fjellvåg, A. Gronvold, T. Fuglerud, J. Hafizovic, O. B. Vistad, D. Akporiaye, J. Catal. 2009, 268, 290.
[221] D. S. Wragg, D. Akporiaye, H. Fjellvåg, J. Catal. 2011, 279, 397.
[222] S. M. Maier, A. Jentys, J. A. Lercher, J. Phys. Chem. C 2011, 115, 8005.
[223] J. K. Norskov, T. Bligaard, J. Rossmeisl, C. H. Christensen, Nat. Chem. 2009, 1, 37.
[224] D. A. Simonetti, J. H. Ahn, E. Iglesia, J. Catal. 2011, 277, 173.